

Tectonics

RESEARCH ARTICLE

10.1029/2019TC005503

Key Points:

- There is an ~8-km-long discontinuous ground rupture within an ~50-km-long, ~12-km-wide zone of uplift based on SAR pixel offset analysis
- Trenching reveals NE striking, SE dipping fault strands of the NBF that represent at least one or two pre-2013 surface rupturing events

Supporting Information:

- Supporting Information S1
- Table S1

Correspondence to:

J. M. Rimando,
jeremy.rimando@mail.utoronto.ca

Citation:

Rimando, J. M., Aurelio, M. A., Dianala, J. D. B., Taguibao, K. J. L., Agustin, K. M. C., Berador, A. E. G., & Vasquez, A. A. (2019). Coseismic ground rupture of the 15 October 2013 magnitude (M_W) 7.2 Bohol earthquake, Bohol Island, central Philippines. *Tectonics*, 38, 2558–2580. <https://doi.org/10.1029/2019TC005503>

Received 24 JAN 2019

Accepted 28 JUN 2019

Accepted article online 16 JUL 2019

Published online 1 AUG 2019

Corrected 10 DEC 2020

This article was corrected on 10 DEC 2020. See the end of the full text for details.

Coseismic Ground Rupture of the 15 October 2013 Magnitude (M_W) 7.2 Bohol Earthquake, Bohol Island, Central Philippines

Jeremy M. Rimando^{1,2} , Mario A. Aurelio¹ , John Dale B. Dianala^{1,3} , Kristine Joy L. Taguibao^{1,4} , Krissen Marie C. Agustin^{1,5} , Al Emil G. Berador⁶, and Adriann A. Vasquez⁷

¹National Institute of Geological Sciences, University of the Philippines, Diliman, Quezon City, Philippines, ²Now at the Department of Earth Sciences, University of Toronto, Toronto, Ontario, Canada, ³Now at the Department of Earth Sciences, University of Oxford, Oxford, UK, ⁴Now at the Department of Earth Science and Technology, Akita University, Akita City, Japan, ⁵Now at the Mines and Geosciences Bureau (Region 2), Tuguegarao City, Philippines, ⁶Mines and Geosciences Bureau (Region 7), Mandaue City, Philippines, ⁷PetroEnergy Resources Corporation, Pasig City, Philippines

Abstract The 15 October 2013 magnitude (M_W) 7.2 Bohol earthquake produced an ~50-km-long, ~12-km-wide northeast trending zone of uplift with an ~8-km-long discontinuous ground rupture indicating predominantly reverse-slip movement on a southeast dipping fault. Documentation of the nearly continuous northern terminus of the 2013 Bohol earthquake ground rupture revealed its association to preexisting scarps of the previously unmapped, Quaternary-active North Bohol Fault. Trenching across the rupture at four sites not only reveals the geometry and kinematics of the fault but also shows at least one or two pre-2013 surface rupturing events. Onshore geologic mapping and offshore seismic reflection profiles demonstrate the presence of an island-wide, northeast-southwest trending fold-and-thrust belt through which deformation related to the regional shortening across the Visayan Sea Basin in the central Philippines is likely distributed.

1. Introduction

On 15 October 2013 (8:12 a.m., UTC +8), the island of Bohol in Central Philippines (Figures 1a and 1b) was shaken by a devastating magnitude (M_W) 7.2 earthquake (Figure 1b). The epicenter was located 30 km NE of Tagbilaran (9.86°N, 124.06°E) and had a shallow focal depth (~12 km; Figures 1b and 1c). The earthquake was initially thought to be caused by movement along the East Bohol Fault (EBF; Figure 2), which was the only known active fault on the island prior to the 2013 earthquake. However, rapid response to the earthquake showed the location of the surface rupture of the earthquake 35 km north of the EBF (Bacolcol et al., 2013). More and improved seismicity and field data helped in coming up with a more constrained geometry and location of the earthquake generator. Focal mechanism solutions (FMS) from the Global Centroid Moment Tensor (GCMT) (Dziewonski et al., 1981; Ekström et al., 2012), National Research Institute for Earth Science and Disaster Resilience (NIED) (2013), U.S. Geological Survey (USGS) (2013), and aftershock distribution from the Philippine Institute of Volcanology and Seismology (PHIVOLCS; Philippine Institute of Volcanology and Seismology, 2014) are all consistent with reverse faulting along a fault plane that generally strikes N40–60°E and dips about 45° to the SE (Figures 1b and 1c). All of this information guided the search for the ground rupture in an area where there was previously no mapped active fault.

A relatively continuous, 6-km-long segment of the ground rupture, which was found initially almost a week after the earthquake, is located in the northern sector of the island, in the municipalities of Inabanga and Buenavista (Figure 2). The ground rupture was named by PHIVOLCS as the North Bohol Fault (NBF; Bacolcol et al., 2013) and is also referred to by other researchers as the Inabanga Fault (Felix, 2017; Felix et al., 2014; Lagmay & Eco, 2014).

The 2013 Bohol earthquake is a significant event for the following reasons: (1) it is considered as the historically strongest earthquake to hit the island of Bohol, (2) it was generated by a previously unmapped reverse fault, and (3) it provides valuable information on reverse fault ground rupture since there is a rarity in documented surface faulting associated to reverse fault-generated earthquakes, not only in the Philippines but also worldwide (Rimando, 2015).

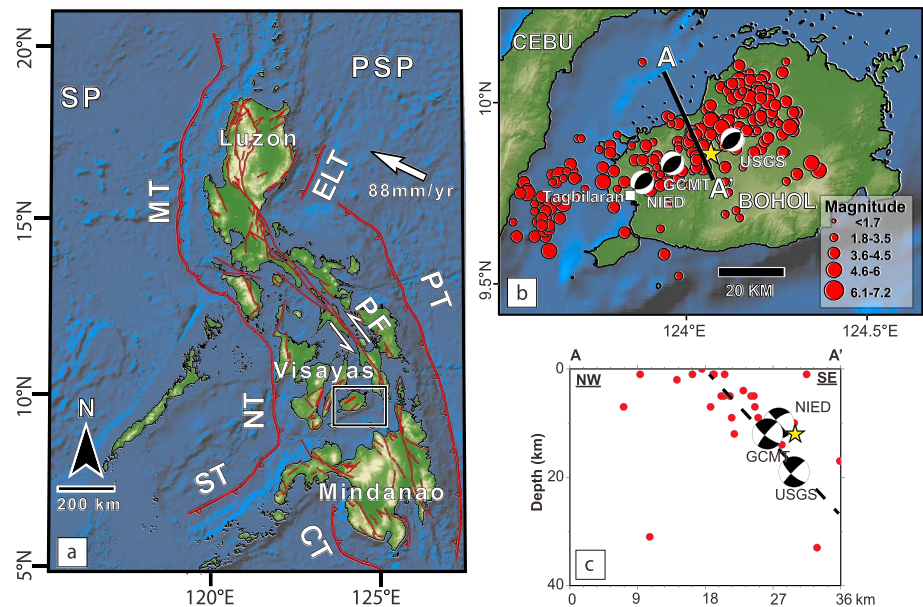


Figure 1. Philippine active tectonic features and seismotectonics of the 2013 Bohol earthquake. (a) Map of tectonic plates (SP = Sunda Plate and PSP = Philippine Sea Plate) trenches (MT = Manila Trench, NT = Negros Trench, ST = Sulu Trench, CT = Cotabato Trench, ELT = East Luzon Trough, and PT = Philippine Trench) and major active faults (e.g., PF = Philippine Fault) in the Philippines modified from PHIVOLCS' Active Faults and Trenches Maps (Philippine Institute of Volcanology and Seismology, 2008). Black box in the Visayas region indicates the location of the study area shown in (b). (b) Map of Bohol island with focal mechanism solutions (FMS) from the Global Centroid Moment Tensor (GCMT), National Research Institute for Earth Science and Disaster Resilience (NIED), and U.S. Geological Survey (USGS); and epicentral locations for the main earthquake event (yellow star) and aftershocks (red circles) from the local seismic network of the Philippine Institute of Volcanology and Seismology (PHIVOLCS). White box indicates the location of Tagbilaran, the capital of Bohol and the black line indicates the location of (c). (c). Sectional view of the seismicity data from different agencies all indicating a SE dipping reverse faulting mechanism for the 2013 earthquake.

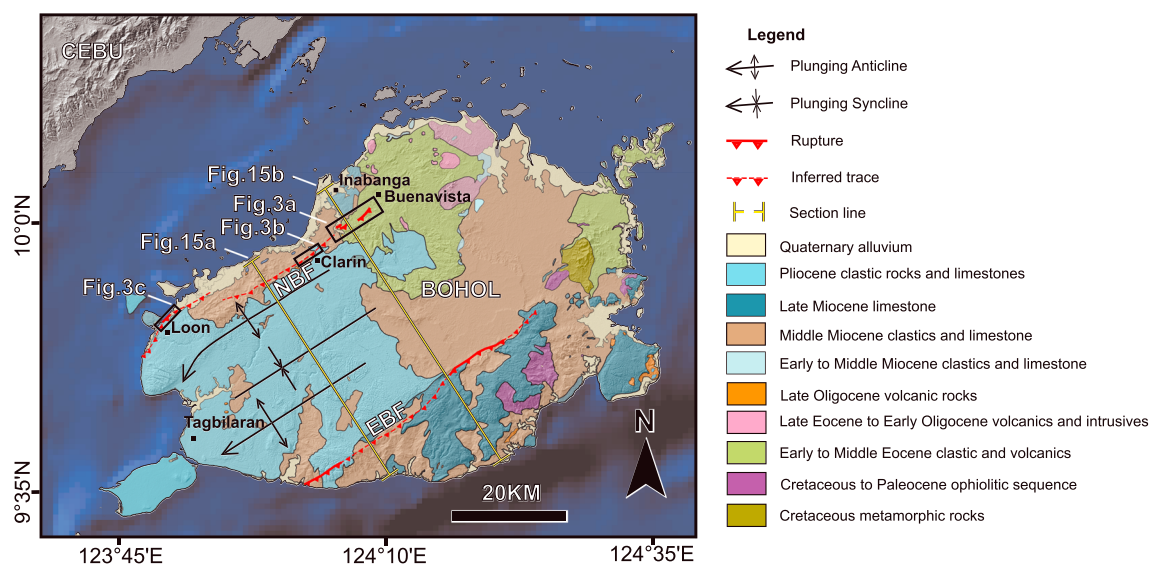


Figure 2. Geologic map of Bohol. Map showing the distribution of different formations and the locations of the North Bohol Fault (NBF), the East Bohol Fault (EBF), and other major structures (modified from the geologic maps of Bureau of Mines and Geosciences (1987) and Metal Mining Agency of Japan-Japan International Cooperation Agency (1985) and the active faults map of Philippine Institute of Volcanology and Seismology (2008). Locations of strip maps of the NBF and geologic cross sections are also indicated.

There is no known existing study yet offering a detailed and comprehensive explanation of the kinematics and activity of the previously unmapped NBF. The primary interest of this paper, therefore, is to discuss the results of (1) ground rupture mapping, (2) paleoseismic trenching, (3) onshore geological mapping, and (4) offshore 3-D seismic profile interpretation. This information will help answer questions regarding the NBF's kinematics and activity and the relation of these to the island-scale structures and its regional geodynamic setting.

2. Tectonic Setting

Bohol Island is situated to the north of Mindanao, the southernmost and second largest island in the Philippines (Figures 1a and 1b). The Philippine Archipelago is mostly an island arc sandwiched to the west by the east dipping Manila-Negros-Sulu-Cotabato Trench System and to the east by the west dipping East Luzon Trough-Philippine Trench System, along which the subduction of the Sunda Plate and the Philippine Sea Plate, respectively, take place (Hamilton, 1979; Acharya & Aggarwal, 1980; Bautista et al., 2001; Cardwell et al., 1980; Hamburger et al., 1983; Hayes & Lewis, 1985; Ozawa et al., 2004). The oblique convergence between the Philippine Sea Plate and the Sunda Plate is accommodated by slip partitioning in the Philippine region. One component is accommodated by subduction perpendicular to the East Luzon Trough-Philippine Trench System, while the other component is accommodated along strike by the ~1,400-km-long, sinistral strike-slip Philippine Fault Zone (PFZ; Allen, 1962; Hamilton, 1979; Barrier et al., 1991; Aurelio et al., 1991; Aurelio et al., 1994; Aurelio, 2000a, 2000b; Besana & Ando, 2005; Yu et al., 2013). The PFZ runs all along Luzon in the north (up to ~800 km from the northern terminus in Luzon; Bischke et al., 1990; Ringenbach et al., 1993; Nakata et al., 1996; Daligdig, 1997), through central Philippines (~800–1,100 km; Aurelio et al., 1991; Aurelio et al., 1997; Besana & Ando, 2005), and southward to Mindanao (1,100–1,400 km; Pubellier et al., 1994; Quebral et al., 1996; Figure 1a).

The major regional structures in the vicinity of Bohol Island are the Negros Trench and the central and southern segments of the PFZ (Figure 1a).

3. Coseismic Ground Rupture

3.1. Rupture Trace

Field investigations were carried out to characterize the nature of ground deformation features associated with the 2013 earthquake. Other possible phenomena that could produce these scarps such as large-scale, deep-seated landsliding and secondary faulting are unlikely. For instance, the absence of landslides uphill of the mapped surface break clearly indicates that these deformational features could not be landslide-toe scarps. Secondary faulting related to backthrusting and flexural slip faulting is not consistent with the seismicity (Figures 1b and 1c), preexisting topography and rupture trace (Figure 3), and the geology of the area (Figure 2).

Moreover, scarp morphologies and complexity of fault trace patterns observed are comparable to ground ruptures of recent earthquakes with significant reverse/thrust component such as the (1) M_W 7.6 1999 Chi-Chi, Taiwan, earthquake (Lin et al., 2001); (2) M_W 7.6 2005 Kashmir earthquake in Pakistan (Kaneda et al., 2008); (3) M_W 7.9 2008 Wenchuan (Sichuan) earthquake in China (Liu-Zeng et al., 2009; Tan et al., 2012); and (4) M_W 7.7 2013 Balochistan, Pakistan, earthquake (Vallage et al., 2015). The discontinuous reverse/thrust ruptures of the M_W 7.2 1992 Suusamy, Kyrgyzstan, earthquake, (Ainscoe et al., 2018) is similar to the 2013 Bohol earthquake rupture.

The ground rupture (Figures 3–6), trending N40–60°E and dipping 50–70°SE, was located in an area with rolling hills topography—along a transition from flat terrain to the mountainous area. Based on seismicity distribution (Figure 1b), it appears that the relatively continuous ground rupture that was documented in the municipalities of Inabanga and Buenavista (Figures 3a and 4) comprises the northeastern portion of the expected entire length of the earthquake generator. Much shorter, and highly discontinuous, traces of the 2013 rupture were also found in the central (Figures 3b and 5) and southwestern portions of the island (Figures 3c and 6).

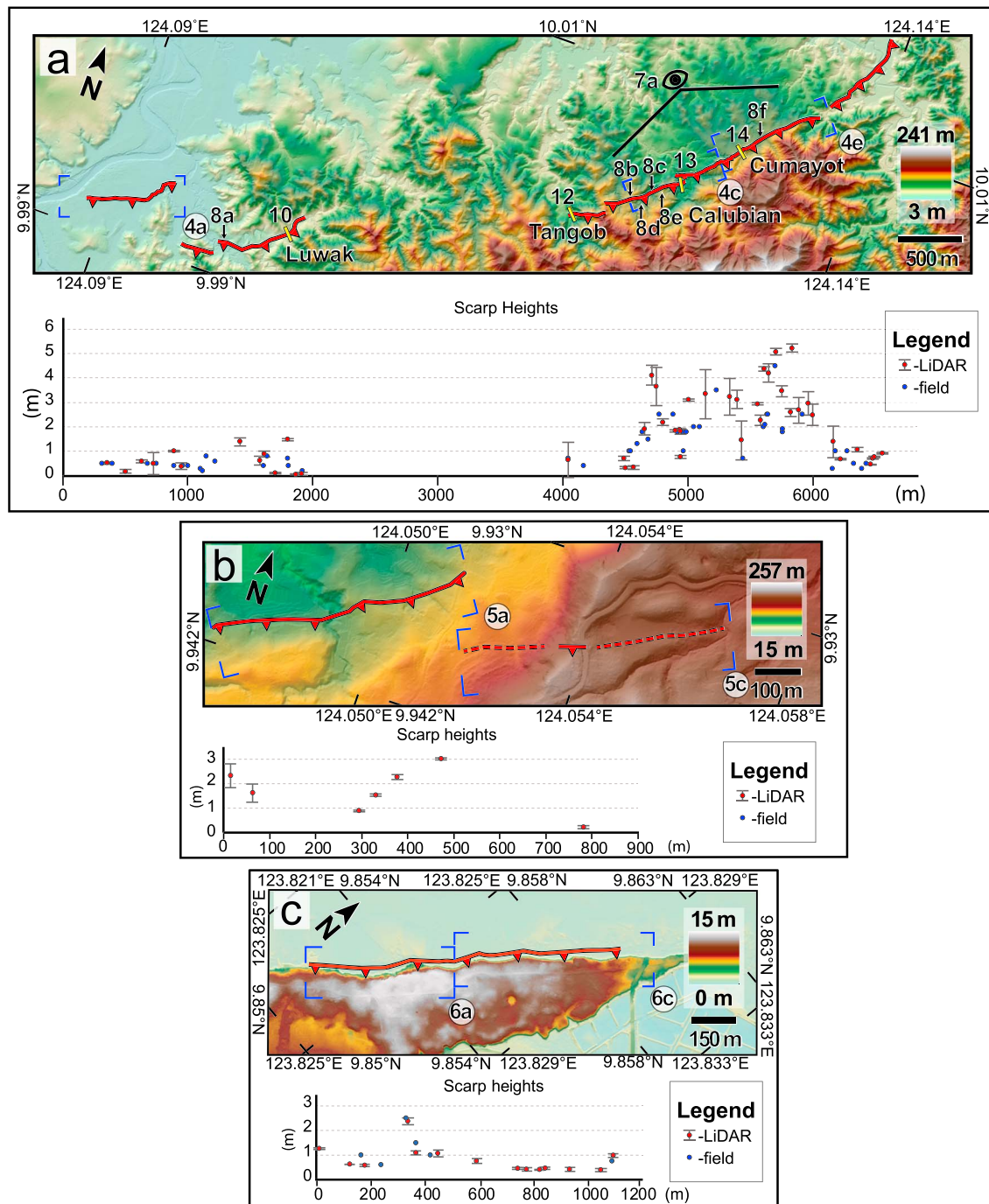


Figure 3. Rupture strip map and scarp height distribution graph. (a) Map of the approximately 6-km-long continuous rupture segment in Inabanga. (b) Map of the less than 1-km rupture in Clarin. (c) Map of the less than 1-km rupture in Loon (see Figure 2 for location). Rupture (indicated by red lines with sawteeth) is plotted on a 1-m resolution (0.5-m vertical and horizontal accuracy) Light Detection and Ranging (LiDAR)-derived digital elevation model. Numbers and number-letter combination labels correspond to other figures. Field- and LiDAR-based scarp height measurements (in meters) along this segment of the NBF are projected onto a graph below. Digital elevation model is from the Philippine-Light Detection and Ranging (Phil-LiDAR) program (University of the Philippines Training Center for Applied Geodesy and Photogrammetry, 2015). Details of scarp heights are listed in Table S1 and shown in Figures S1–18.

3.2. Scarp Height Measurements

Scarp heights were measured both in the field using a tape measure (Figures 3 to 7 and S1 to S9 and Table S1 in the supporting information) and from topographic profiles constructed from 1-m resolution (0.5-m vertical and horizontal accuracy) Light Detection and Ranging (LiDAR) digital elevation models (DEMs;

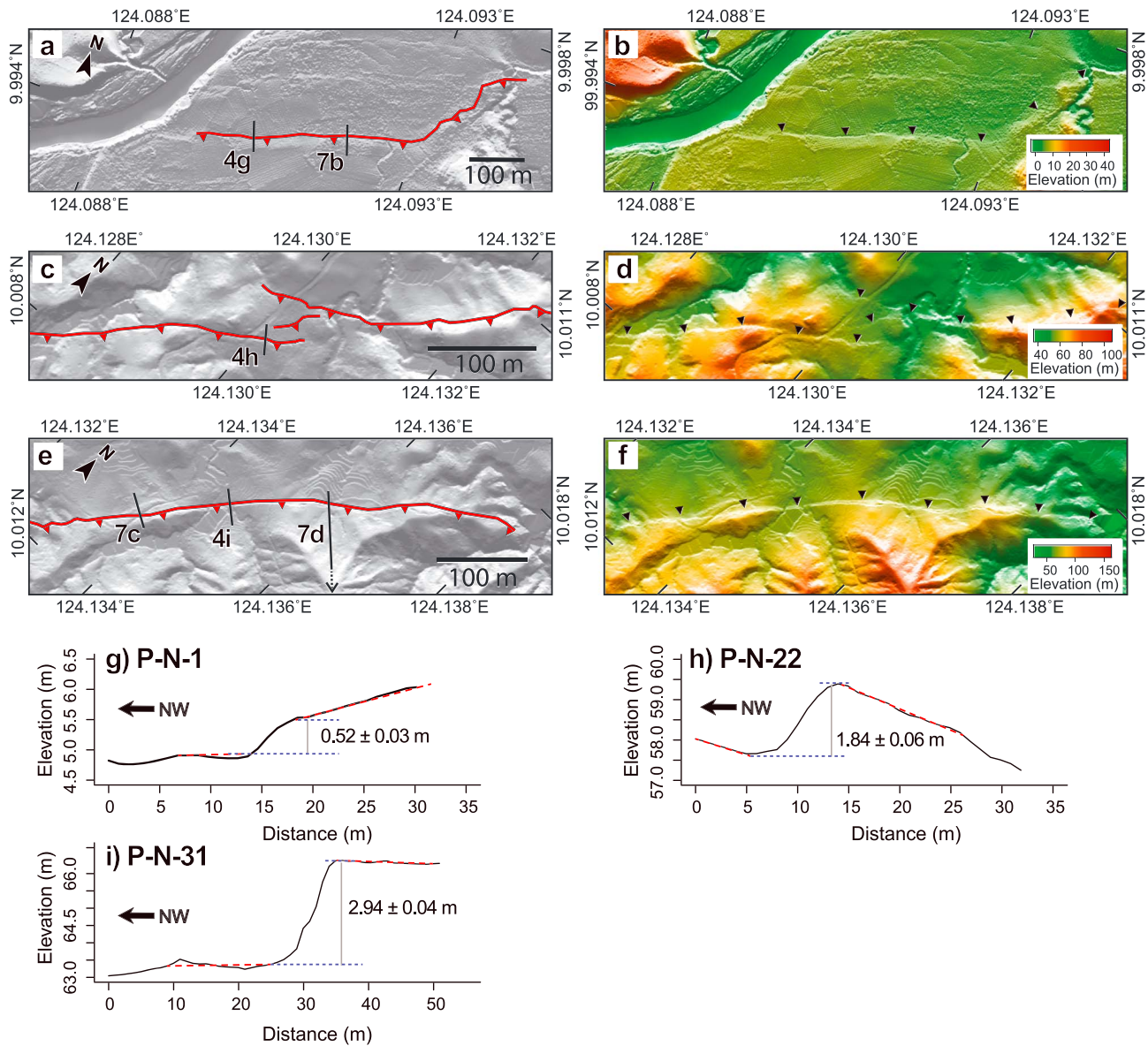


Figure 4. Detailed rupture strip maps of Inabanga. (a, c, and e) Strip maps are annotated with the rupture trace and locations of featured scarp profiles. (b, d, and f) Strip maps are bare digital elevation model-hillshade overlay versions of (a), (c), and (e), with black triangle symbols showing the basis of the trace. Locations of strip map pairs are indicated by blue corners as seen in Figure 3a. (g–i) Examples scarp profiles along this rupture segment.

Figures 3 to 7 and S10 to S18 and Table S1) following a procedure described in Yang et al. (2015). LiDAR data used for these profiles were acquired not too long after the earthquake—between 11 November and 4 December 2013 (University of the Philippines Training Center for Applied Geodesy and Photogrammetry, 2015). Scarp heights along the northeastern segment of the NBF in Inabanga (Figures 3a and 4) are significantly larger in the northeast than in the southwest. In the northeast, scarp heights are mostly 2 m and reach a maximum of 5 m, while in the southwest, scarp height is mostly less than 1 m. The maximum and average scarp heights, which were measured along the nearly continuous approximately 2-km-long ground rupture in Sitio Cumayot, Barangay Anonang, Inabanga, are around 5 and 2 m, respectively.

The continuity and amount of displacement exhibited by this portion of the NBF's 2013 rupture provides an opportunity to document scarp morphology and investigate possible structural or kinematic controls. Two other traces, which were each less than a kilometer long, were documented in the towns of Clarin (Figures 3b and 5) and Loon (Figures 3c and 6). Scarp heights along the segment in Clarin (Figures 3b

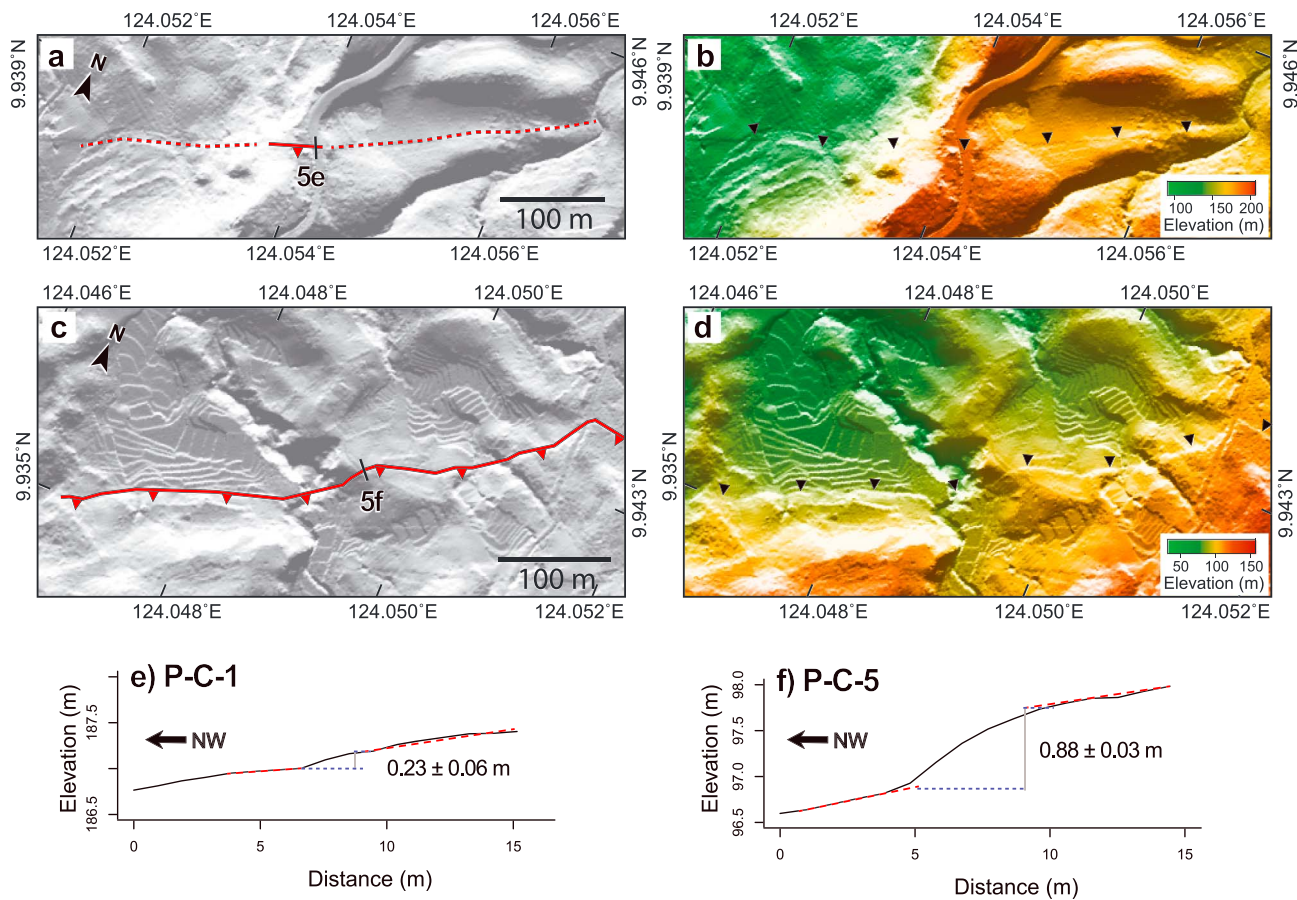


Figure 5. Detailed rupture strip maps of Clarin. (a, c) Strip maps are annotated with the rupture trace and locations of featured scarp profiles. (b, d) Strip maps are bare digital elevation model-hillshade overlay versions of (a) and (c), with black triangle symbols showing the basis of the trace. Locations of strip map pairs are indicated by blue corners as seen in Figure 3b. (e and f) Examples of scarp profiles along this rupture segment.

and 5) were highly variable and were on average around 2 m. Scarp heights in Loon, on the other hand (Figures 3c and 6), were on average less than a meter high.

3.3. Scarp Morphologies

Fault scarps, which exhibit the vertical component of displacement of land as a result of movement along a fault, may have various morphologies along the length of a reverse fault which may result from a variation in amount of slip, sense of slip, the geometry of fault(s), properties of the surficial materials, and preexisting topography of the area (Philip et al., 1992).

Varied scarp morphologies were found along the nearly continuous, longest 2013 ground rupture of the NBF in between the municipalities of Inabanga and Buenavista. Scarp morphologies observed along the 6-km-long rupture in Inabanga include monoclinical fault scarps similar to those observed along the ground rupture of the 2005 M_W 7.6 Kashmir, Pakistan, earthquake (Kaneda et al., 2008) and simple reverse (thrust) fault scarps, hanging wall collapse scarps, sinistral pressure ridges, and low-angle pressure ridges similar to those observed along the ground rupture of the 1988 M_s 6.9 Spitak, Armenia, earthquake (Philip et al., 1992). There were also occurrences of *en echelon* monoclinical fault scarps in areas with distributed slip and of mole-tracks at fault termini where there was very minimal or almost no appreciable vertical displacement. Representative scarp morphologies are shown in Figure 8, and their locations are indicated in the rupture strip map of Figure 3a.

We use the term simple reverse fault scarps after Philip et al. (1992) to describe scarps which exhibit a sharply defined, steeply dipping fault plane. Simple reverse fault scarps (Figure 8f), in general, occur in portions

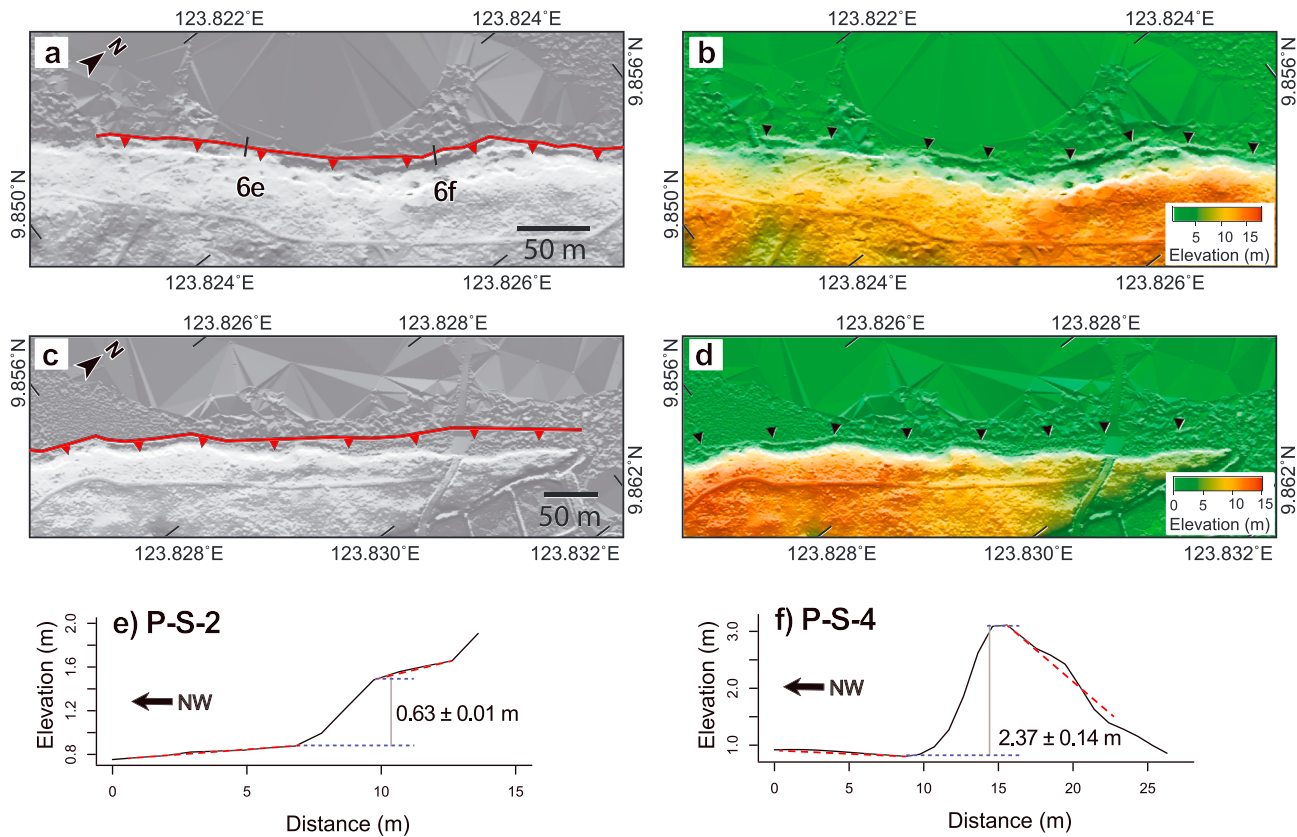


Figure 6. Detailed rupture strip maps of Loon. (a, c) Strip maps are annotated with the rupture trace and locations of featured scarp profiles. (b, d) Strip maps are bare digital elevation model-hillshade overlay versions of (a) and (c), with black triangle symbols showing the basis of the trace. Locations of strip map pairs are indicated by blue corners as seen in Figure 3c. (e and f) Examples of scarp profiles along this rupture segment.

of the rupture with larger vertical separation. However, other scarp morphologies are also observed having large vertical separation. According to Philip et al. (1992), the occurrence of simple reverse fault scarp morphology is more reliant on the near-surface inclination of the fault plane. Simple reverse fault scarps seem to occur where the fault plane is steeply dipping ($>45^\circ$). This type of scarp was observed to occur mostly in the middle portion of the rupture between Sitio Calubian and Sitio Cumayot, Barangay Anonang, Inabanga (Figure 3a). In this area, there is only a thin soil cover on top of the andesitic rocks of the Ubay Formation. The brittle nature of the andesitic rocks in the area allowed the fault plane to maintain its steep inclination until it reached the surface. In areas with a thick layer or sequence of overlying soft substrate (e.g., soil and alluvium), fault refraction usually takes place beginning at the rock-soil interface and tends to result in a gentler fault inclination similar to what Vallage et al. (2015) documented in the Balochistan earthquake rupture.

The term hanging wall collapse scarps, after Philip et al. (1992), refers to scarps in which the overhanging material on the upthrown block have fallen (Figure 8b). Hanging wall collapse scarps are also formed by steeply dipping faults. The only difference is that the material involved is usually unconsolidated. Ground shaking due to aftershocks easily causes the overhanging material to collapse and form this type of scarp. This type of scarp was found mostly along the rupture between Sitio Calubian and Sitio Cumayot, Barangay Anonang, Inabanga (Figure 3a).

Monoclinical fault scarps exhibit varying degrees of surface flexure due to the compression accompanying the movement of the hanging wall over the foot wall (Figure 8c). These may show buckling features like fissures and tension cracks on the hanging wall. This type of scarp typically forms in areas with a relatively thick overlying layer or sequence of soft substrate (e.g., soil and alluvium), because of the gentler near-surface fault dip that occurs due to fault refraction at the rock-soil interface. Monoclinical fault scarps do not seem to have a

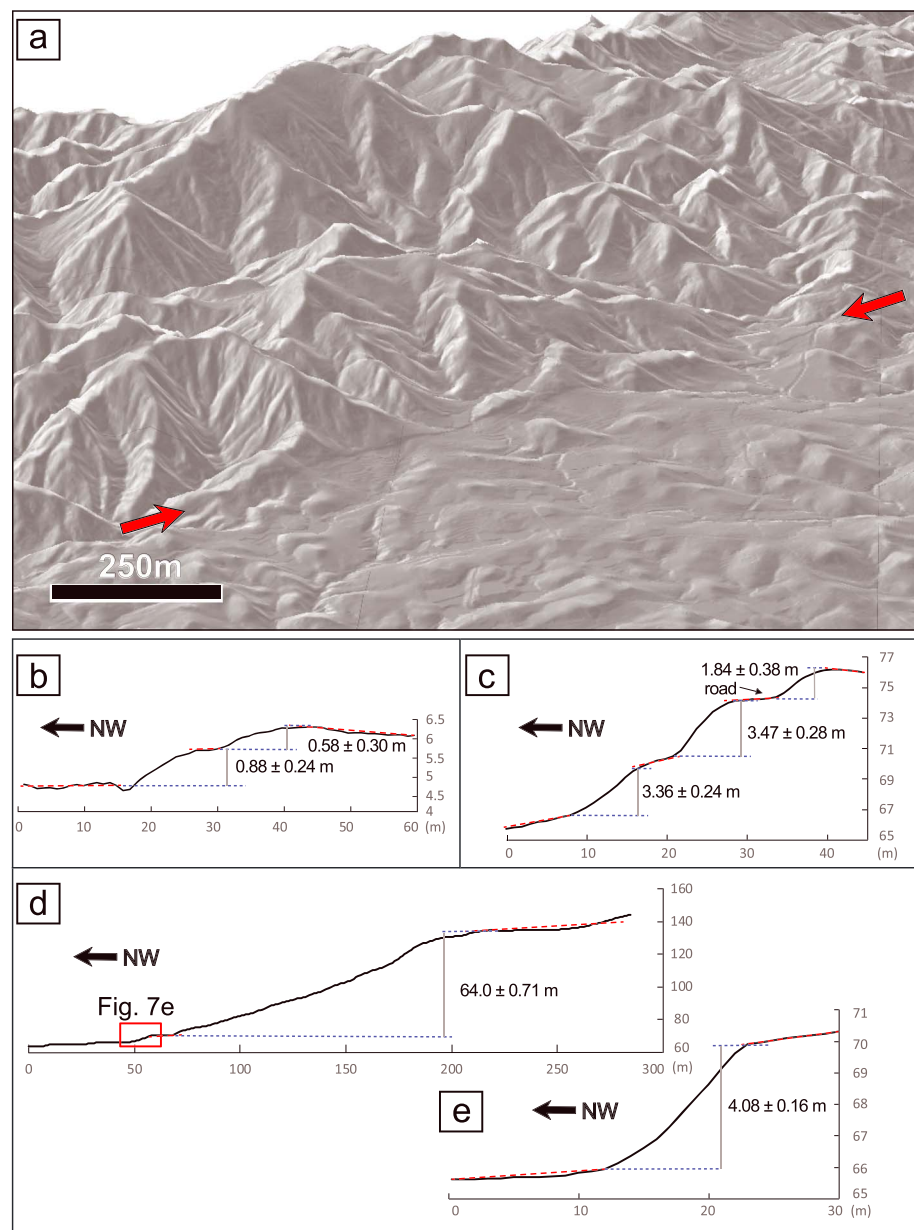


Figure 7. Preexisting morphotectonic features. (a) Oblique view of ground rupture of the North Bohol Fault at the base of the mountainous terrain in Inabanga. Location of this view is shown in Figure 3. Digital elevation model is from a 1-m resolution (0.5-m vertical and horizontal accuracy) Light Detection and Ranging data from the Philippine-Light Detection and Ranging program (University of the Philippines Training Center for Applied Geodesy and Photogrammetry, 2015). (b) Topographic profile of a cumulative scarp showing two events: the ~0.9-m-high 2013 rupture at the base in the northwest and a preexisting scarp to the southeast. Location indicated in Figure 4a. (c) Topographic profile of a cumulative scarp showing possibly at least three events based on average scarp height in this location: the ~3.5-m-high 2013 rupture in the center and preexisting scarps northwest and southeast of it. Location indicated in Figure 4e. (d) Topographic profile of a more than 60-m-high cumulative scarp, with the ~4-m-high 2013 rupture at the base in the northwest (Figure 7e). Location indicated in Figure 4e.

correlation with the amount of vertical separation; these can form with any amount of vertical separation (10–180 cm). However, these are also not observed in portions of the rupture with very large vertical separation (>180 cm). Monoclinical scarps were found mostly due southwest and northeast of the rupture between Sitio Calubian and Sitio Cumayot, Barangay Anonang, Inabanga.



Figure 8. Scarp morphologies. (a) Low-angle pressure ridge. (b) Hanging wall collapse scarp. (c) Monoclinal fault scarp. (d) Sinistral pressure ridge. (e) A series of three left-stepping *en echelon* monoclinical fault scarps. (f) Simple reverse fault. Rupture diagrams below were modified from Philip et al. (1992). See Figure 3a for locations.

En echelon monoclinical fault scarps result from the distribution of slip along several fault planes branching to the surface (Figure 8e). These branching fault planes could be preexisting planes of weakness such as lava flow or bedding planes.

The term sinistral pressure ridges after Philip et al., (1992) describes scarps with *en echelon* tensile cracks within the hanging wall, which form due to oblique slip (Figure 8d). The orientation of these tensile cracks supposedly indicates the sense of slip. Along the 6-km-long (end-to-end) rupture (Figure 3a), only sinistral pressure ridges were observed. The sense of slip reflected by these scarps is consistent with the minor

sinistral component of slip registered by the focal mechanism by the Global Centroid Moment Tensor project. It should be noted, though, that only three scarps observed in this study exhibit a sinistral component of slip—therefore, these cannot be utilized to determine the sense of the lateral component of slip of the entire NBF. These sinistral pressure ridges could, at least, be useful to indicate at least the local sense of lateral slip as lateral slip typically varies in sense and magnitude along strike in reverse/thrust faults. Furthermore, the sinistral component of slip of the scarp needs not be reconciled with the sense of slip indicated in either FMS since these display a very minimal lateral component of slip and since FMS are also prone to error (Hardebeck & Shearer, 2002 and Tape & Tape, 2012). Quantitative description of the lateral component of offset was also not documented due to the lack of reliable measurable offset markers like roads or natural linear features where sinistral pressure ridges were found.

Lastly, low-angle pressure ridges, according to Philip et al. (1992) are scarps that are formed by detachment of a thin, superficial turf layer which in turn forms the gentle folding in front of the reverse/thrust fault (Figure 8a). Low-angle pressure ridges seem to have a correlation with the amount of vertical separation. These are observed along portions of the rupture, which have very small vertical separation—usually toward the ends of the rupture where vertical separation tapers. (Figure 3a). While there is no natural exposure showing a sectional view of this type of scarp, for detachment of a thin turf layer to occur, a very gently dipping fault is more likely to have been involved.

3.4. Preexisting Morphotectonic Features

Locating the ground rupture in the northern sector of Bohol, an area where there was previously no documented active fault trace prior to the earthquake, prompted closer examination of topographic maps and high-resolution DEMs, to identify evidence of prior fault activity. The approximately 6-km-long rupture that was traced in the municipality of Inabanga appears to be aligned to faceted mountain spurs or preexisting scarps (Figures 7a–7d)—which seemed to have formed as a result of cumulative displacement along the NBF. These features, however, are subtler compared to those which were used to indicate activity and kinematics of other faults in the Philippines, such as along the Philippine Fault (Nakata et al., 1977; Nakata et al., 1996; Rimando & Knuepfer, 2006; Tsutsumi et al., 2015) and the Marikina Valley Fault System (Rimando & Knuepfer, 2006). For instance, Rimando and Knuepfer (2006) documented long, continuous, preexisting fault traces (as much as 115-km-long rupture segments) along the Marikina Valley Fault System with ~3.4-m-high maximum single-event scarps and 250-m-high cumulative scarps, which were prominent and preserved well enough to allow estimation of the possible number events that formed these preexisting cumulative scarps.

Nonetheless, these morphotectonic features still indicate relative recency of movement of the preexisting fault since existence of such cumulative scarps suggest rates of tectonic activity at least surpass rates of erosion, which can be exceptionally high especially in a tropical country like the Philippines, that experiences regular heavy monsoon- and frequent typhoon-related rains.

4. Trench Exposures

Four trenches, Luwak, Tangob, Calubian, and Cumayot (Figures 3a, 10, and 12–14), 2, 1, and 0.5 km apart, respectively, were excavated across the Inabanga segment of the NBF to identify and characterize its prehistoric activity. This is the first paleoseismic trenching investigation in the island of Bohol and on any reverse fault in the Philippines. Trenches were named after the *sitio* (literally “site,” a division of a barangay or village, the smallest government unit in the Philippines).

The Luwak Trench is situated in a valley formed by parallel northeast-southwest oriented ridges (Figure 9a) and is found in Sitio Luwak, Barangay Napo, in the municipality of Inabanga. It is located east of the Luwak creek. The type of scarp in the Luwak Trench site is monoclinical, approximately 70 cm high, and oriented N40°E. The Tangob Trench (Figure 9b) is found in Sitio Tangob, Barangay Liloan Norte in the municipality of Inabanga. The type of scarp in the Tangob Trench site is monoclinical, approximately 70 cm high, and oriented N60°E. It is located east of the Tangob creek and at the southwestern edge of a northwest trending valley where the Tangob creek flows. It is in an area exhibiting sudden change in relief from low lying to hilly terrain. The Calubian Trench (Figure 9c) is found in Sitio Calubian, Barangay Anonang in the municipality of Inabanga. The trench is situated in the transition between gently sloping land from the mountainous area.

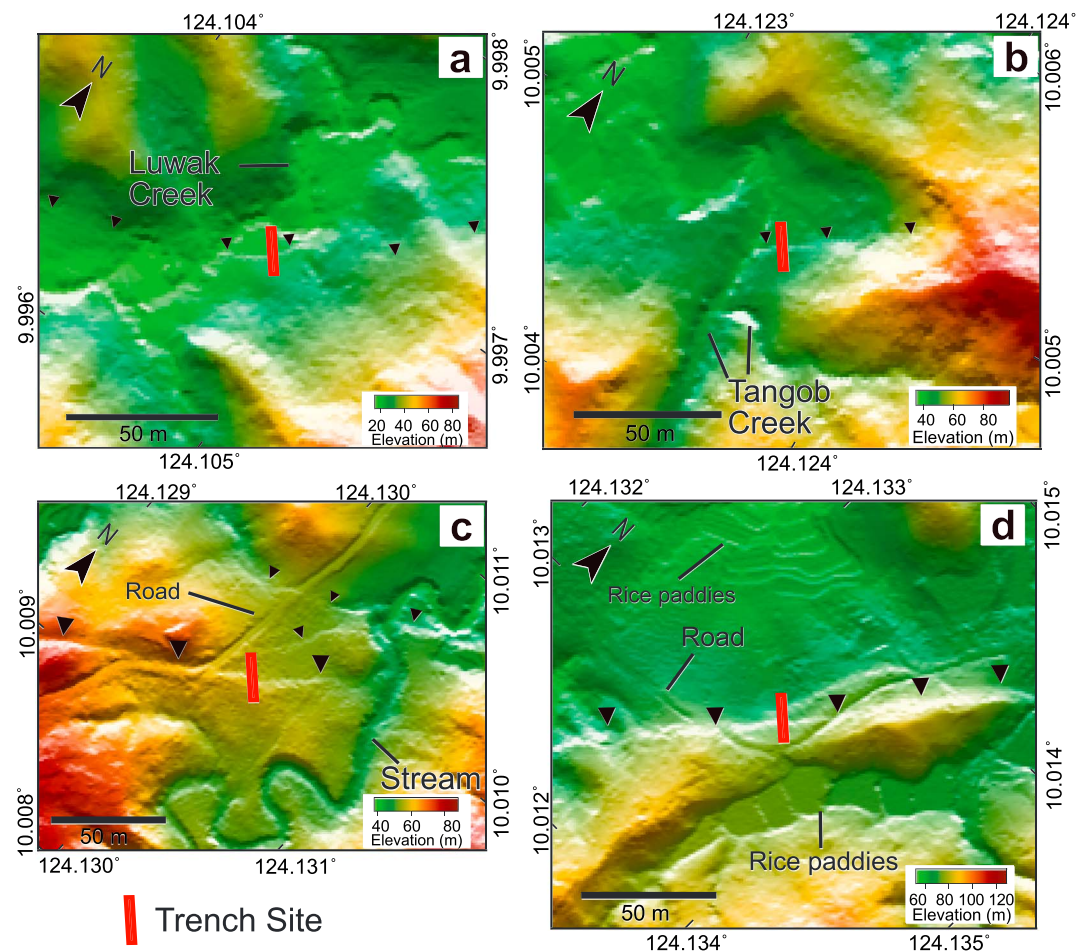


Figure 9. Trench location maps. (a) Luwak Trench. (b) Tangob Trench. (c) Calubian Trench. (d) Cumayot Trench. Location of these trenches along the ground rupture in Inabanga can be seen in Figure 3a.

The type of scarp in the Calubian Trench site is a sinistral pressure ridge, approximately 180 cm high, and oriented N50°E. The Cumayot Trench (Figure 9d) is found in Sitio Cumayot, Barangay Anonang in the municipality of Inabanga, is only 500 m northeast of Calubian Trench. The type of scarp in the Cumayot Trench site is monoclinical, approximately 150 cm high, and oriented N40°E.

Finding ideal trench locations proved challenging. In the southwestern end of the rupture of Figure 3a, where there was a potential for recovering a lot of organic material land was heavily and deeply plowed for different crops and had a very shallow water table. There was also difficulty with securing permission from land owners, as those areas are farm land, which owners were not willing to be disrupted.

In the remote Luwak and Tangob Trench sites, where the only access is by foot, trenches were manually excavated. In the Calubian and Cumayot Trench sites, where there are access roads, a backhoe was used for excavation. The northeastern and southwestern walls of the trenches were logged at a scale of 1:25 using mosaics of photos taken perpendicular to the trench wall. Wood, charcoal, and organic sediment/*gytija* were collected for accelerator mass spectrometry radiocarbon dating at Beta Analytic Laboratory in Miami, Florida, USA.

The stratigraphy and the basis for identifying paleoseismic events in each trench are described in the following sections. Layers were named “Unit,” followed by a number (1, 2 ... n) from youngest to oldest. The letter “F” and “S” were used to indicate “fault” and “sample,” respectively; an initial or first two letters of the sitio to indicate the trench name (“L” for Luwak, “T” for Tangob, “Ca” for Calubian, and “Cu” for Cumayot); the letter “N” or “S” to indicate either “northeast” or “southwest” wall; and a number to indicate relative age (1, 2 ... n) from youngest to oldest.

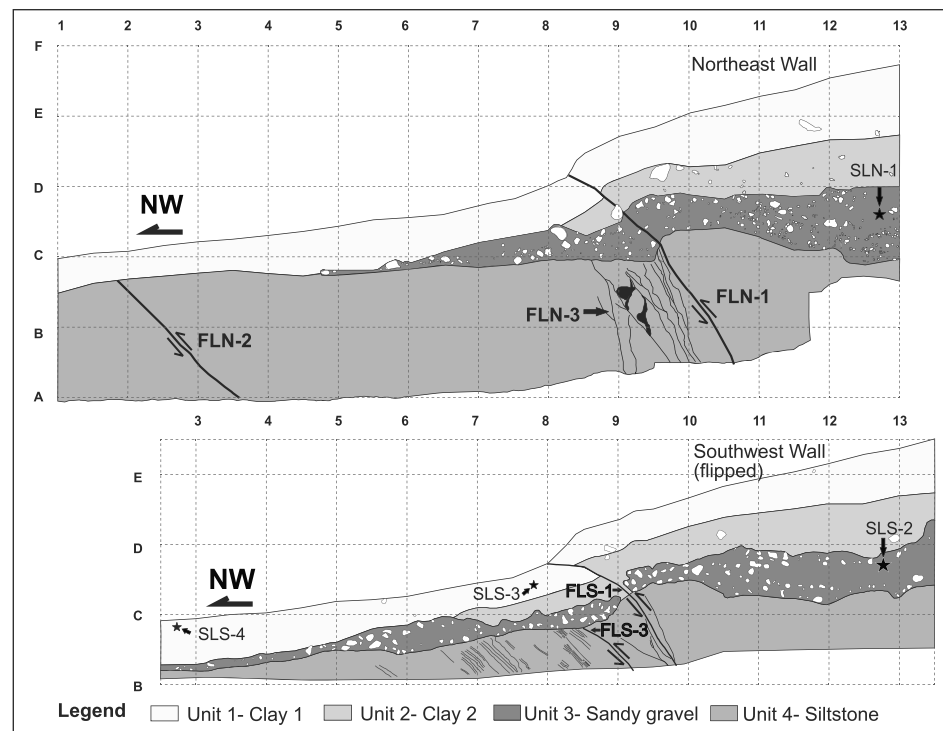


Figure 10. Luwak Trench interpretation. Grids are spaced 1 m. See supporting information Figure S19 for photomosaic.

4.1. Luwak Trench

The 12-m-long and 2.5-m-wide benched Luwak Trench (Figure 10; labeled “10” in Figure 3a), situated in a northeast-southwest oriented stream valley, was excavated across a 0.50-m-high monoclinical fault scarp. The northeastern wall reached a depth of 3.7 m in one portion while the southwestern wall reached a depth of about 3 m.

4.1.1. Stratigraphy of Luwak Trench

Four stratigraphic units were identified in both trench walls of Luwak Trench. Three upper units are unconsolidated deposits, while the fourth and oldest is bedrock. The units are described below in detail in order of relative age (Unit 1 being the youngest unit; Figure 10).

Unit 4 is sandy siltstone. The portion of the bedrock on the upthrown block has been repeatedly uplifted and preferentially weathered by oxidation. This unit is overlain by Unit 3. Unit 3 is a loose, unconsolidated deposit of pebble-cobble-sized andesite clasts set in a sandy-silty matrix of intermediate composition (Figure 10). The layer is matrix supported. Compositionally, the proportion of the different components in this layer include 60% sandy-silt matrix, 30% pebbles, and 10% cobbles. The thickness of this unit varies significantly along the trench wall, with thickness ranging from about 10 cm to 1 m. The lithology of the clasts and the matrix of this layer show no semblance to the bedrock beneath and the soil above, respectively, and so it must have been sourced distally. There are several possible origins for this deposit: an alluvial strath terrace that was abandoned following coseismic uplift, talus due to intense shaking from an uphill source, or colluvium from a previous uphill scarp. Due to the uncertainty in the origin of this deposit, we call it a “sandy gravel” layer to avoid any genetic implication. Unit 2 is a very cohesive clay soil layer (Figure 10) with minimal amount of andesitic pebble to cobble clasts and which is barren of datable organic matter. Unit 2 is most likely a transported soil due to the lack of a saprolite layer, which would indicate alteration/weathering of the layer beneath. Some pebbles from the sandy gravel layer were likely incorporated into the soils as the soil was being transported downslope. It overlies Unit 3 and tapers toward the downthrown portion of the trench. Variation in thickness of this unit ranges from 50 to 75 cm. Whether this unit comprises colluvium that was coseismically deposited from an uphill source is uncertain. The thinning out of Units 2 and 3 in the Luwak Trench is due to the trench location being at the base of topography with very minimal sediment

Table 1
Radiocarbon Dating Results

Beta code	Sample name	Source layer	Conventional radiocarbon age	Calendar calibrated age ^a	Material type
Beta-383129	SLN-1	Unit 3 (Luwak)	10650 ± 40 BP	Cal BC 10,745 to 10,610 (Cal BP 12,695 to 12,560)	Organic sediment
Beta-383130	SLS-2	Unit 3 (Luwak)	10930 ± 40 BP	Cal BC 10,875 to 10,775 (Cal BP 12,825 to 12,725)	Organic sediment
Beta-382121	SLS-3	Unit 1 (Luwak)	50 ± 30 BP	Cal CE 1,695 to 1,725 (Cal BP 255 to 225) and Cal CE 1,815 to 1,835 (Cal BP 135 to 115) and Cal CE 1,880 to 1,915 (Cal BP 70 to 35) and Post CE 1950 (Post BP 0);	Charred material
Beta-382119	SLS-4	Unit 1 (Luwak)	146.7 ± 0.4 pMC	NA	Charred material

Note. BP = before “present”; “Present” = CE 1950; CE = Common Era; pMC = percent modern carbon units; “pMC” indicates that the analyzed material had more ¹⁴C than did the modern (CE 1950) reference standard which is most probably caused by introduction of “extra” ¹⁴C in the atmosphere from thermonuclear bomb testing, which began in the 1950s. NA = not applicable.

^aRefers to the calendar ages obtained from calibration of the 2-sigma range of the conventional (measured) radiocarbon ages (fourth column) against the INTCAL13 database (supporting information Figures S3–S25; Reimer, et al., 2013).

input. Unit 1 is a very cohesive clay topsoil (Figure 10). This layer overlies Unit 2, except toward the downthrown portion of the northeastern trench wall where Unit 2 thins out. Variation in thickness of this unit is minimal, with thickness ranging from 50 to 75 cm. Warping and variation in the thicknesses of Units 2 and 1 due to the rupture could be observed. Between Unit 1 and Unit 2, there seems to be a gradational contact suggesting at least some of the portions of Unit 1 developed from Unit 2. The larger extent of Unit 1, however, suggests that some of the soil is also transported.

4.1.2. C-14 Dating of Organic Material in Luwak Trench

Two samples of charred wood from Unit 1 were sent to Beta Analytic for accelerator mass spectrometry radiocarbon dating—SLS-3 (Beta 382121) and SLS-4 (Beta 382119; Figure 10; Table 1). SLS-4 was reported with “pMC,” indicating that the material analyzed was most likely respired carbon after the beginning of thermonuclear bomb testing circa 1950. (Table 1). The young ¹⁴C ages of SLS-3 and SLS-4 obtained are most likely younger plant parts that were incorporated into inconspicuous mudcracks in the clay soil.

Two samples, Beta-383130 (SLN-1) and Beta-383129 (SLS-2), were recovered in two isolated spots from the northeast and southwest trench walls (Figure 10 and Table 1). While SLN-1 and SLS-2, which were recovered in relatively large amounts from the sandy-silt matrix of Unit 3, are officially classified as organic material (organic sediment or gyttja), these had vestiges of woody/fibrous texture upon retrieval/prior to submission to Beta Analytic. These were possibly classified as bulk organic material probably due to their fragility and their tendency to easily breakdown to smaller particles. The similarity in age would support these being deposited material. Combined recalibration of the conventional ages of SLN-1 and SLS-2 against the IntCal13 calibration curve (Reimer et al., 2004) and Bayesian analysis to obtain upper and lower limit age boundaries for Unit 3 using OxCal (<https://c14.arch.ox.ac.uk/oxcal.html>; Bronk Ramsey, 2009) yielded a mean lower boundary age of 13,019 cal BP and a mean upper boundary age of 12,373 cal BP (see Figure S26), which is consistent with a pre-12,000 BP age for Unit 3.

4.1.3. Evidence of Faulting in Luwak Trench

Fault 1 or the 2013 event (“FLN-1” or “FLS-1” in Figure 10) is oriented N40°E. The dip of this fault strand varies from bottom to top: It dips 55°SE through the bedrock (Unit 4), 40°SE through the sandy gravel layer (Unit 3), 30°SE through clay soil (Unit 2) and appears horizontal through the topsoil (Unit 1; FLS-1 in Figure 10). Fault 2, oriented N80°E, 45°SE and found 7 m to the southeast of FLN-1, cuts only the bedrock on the downthrown block of northeast wall (“FLN-2” in Figure 10) and terminates at the contact with the topsoil (Unit 1). Whether this represents manifestation of an even older event is ambiguous as its termination at the base of Unit 1 (and not Unit 2 or 3) could be the effect of either erosion or nondeposition of the Units 2 and 3 in this portion. Very lightly imprinted slickenlines (Figure 11) were observed in the continuation of FLN-2 in the unlogged, benched portion of the SW wall of Luwak Trench. Logging was difficult in the lower portion of the SW wall of the Luwak Trench because of water springing from this side. The orientation of the slickenlines (S10°E, 90° pitch) is exactly vertical, suggesting a pure thrust component of movement for

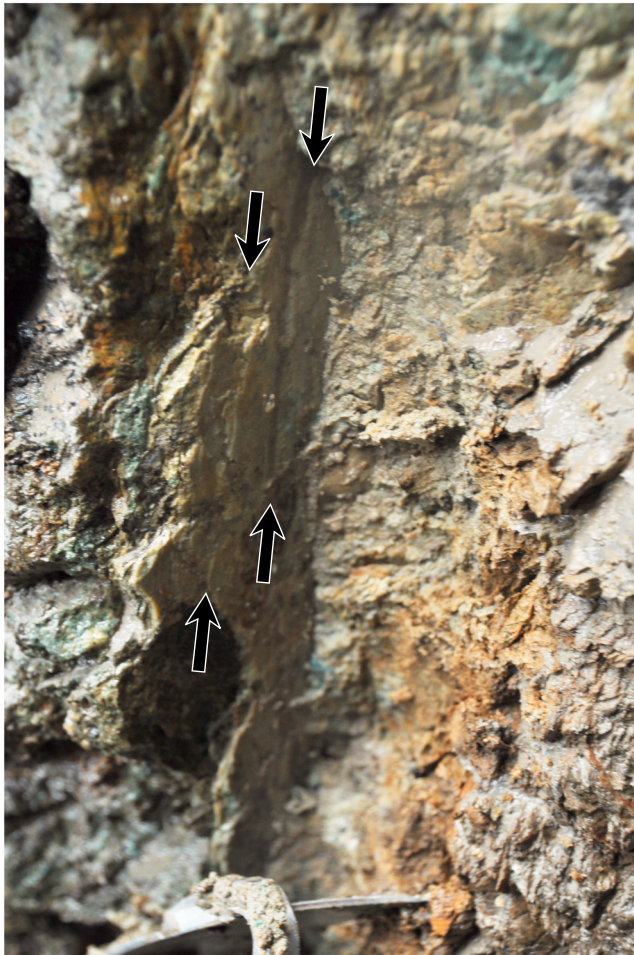


Figure 11. Slickenlines-oriented S10°E (pitch = 90°) observed in continuation of plane of Fault 2 (FLN-2) on unlogged, benched portion of SW wall of Luwak Trench.

one of the pre-2013 events. Fault 3, the oldest identifiable earthquake event, is represented by fault strands oriented N40°E, 55°SE (“FLN-3” or “FLS-3” in Figure 10), which are proximal to FLN-1 or FLS-1, and which profusely cut the bedrock unit but terminate at the base of the sandy gravel layer (Unit 3). Faults are identified by the presence of fault gouge, presence of shearing-related foliation, and presence of sigmoidal deformation features. A possible minimum age of the latest earthquake event associated with FLN-3 or FLS-3, which may have happened before the deposition of the sandy gravel layer, could be constrained by organic material obtained within Unit 3 that caps this event (SLN-1 or SLS-2 in Figure 10 and Table 1).

4.2. Tangob Trench

The 9.5-m-long, 3-m-deep, and 2-m-wide single-slot-style Tangob Trench (Figure 12; labeled “12” in Figure 3a) was excavated across a 0.75-m-high monoclinical fault scarp.

4.2.1. Stratigraphy of Tangob Trench

Five stratigraphic units were identified in both trench walls. Three units are unconsolidated deposits, while two are bedrock. The units are described in detail in order of relative age (Unit 1 being the youngest unit; Figure 12).

The bedrock is composed of two groups of lithologies: Unit 4—alternating beds of sandstone and siltstone that are dipping gently to the NW and Unit 5—weathered and fresh exposures of andesite (Figure 12). These lithologies are juxtaposed along the thrust fault. The alternating beds of sandstone and siltstone are found on the downthrown block, while the andesite which exhibits varied degrees of weathering is found both on the upthrown and downthrown block. These units are unconformably overlain by Unit 3. Unit 3 is a loose, unconsolidated deposit of pebble-boulder-sized andesite clasts set in a sandy-silt matrix of intermediate composition (Figure 12). The layer is matrix supported. The following is the proportion of the different components in this layer: 80% sandy-silt matrix, 15% pebbles, and 5% cobbles. The thickness of this unit varies significantly along the trench wall, with thickness ranging from about 40 to

90 cm. This sandy gravel layer can be correlated with Unit 3 exposed in the Luwak Trench, which, similarly, has uncertain origin. Unit 2 is very cohesive clay soil layer barren of datable organic matter (Figure 12). It overlies Unit 3. Similar to Unit 2 in Luwak Trench, this is also likely a transported soil. Thickness of this unit varies substantially from 30 to 85 cm. Unit 1 is topsoil (Figure 12). It is a cohesive clay soil barren of datable organic matter which is almost uniformly 30 cm thick, except for the portion where the scarp formed (up to 80 cm thick). This layer conformably overlies Unit 2. Similar to Luwak Trench, Unit 1 seems to have developed from Unit 2 and has been enriched in organics. Warping and variation in the thicknesses of Units 1 and 2 due to the rupture could be observed.

4.2.2. Evidence of Faulting

Fault 1 (“FTN-1” or “FTS-1” in Figure 12), the fault strand associated with the 2013 event, is oriented N60°E. The dip of this fault strand varies from the bottom to the top: It dips 65°SE through the bedrock (Units 4 and 5); 45°SE from the top of the bedrock until midway through the sandy gravel layer (Unit 3); 30°SE up to the clay soil (Unit 2), and nearly horizontal at the topsoil layer (Unit 1). Tension cracks as wide as 40 cm, which penetrate the sandy gravel layer are associated with this most recent earthquake (Figure 12). The cluster of tension cracks are found 2 m behind the fault scarp and span about 1.5 m. Fault 2 (“FTN-2” or “FTS-2”) is a group of strands which cut both the bedrock and the sandy gravel layer on the downthrown side of Fault 1. FTN-2/FTS-2 is oriented N60–70°E, 45°SE and exhibits as much as 25-cm vertical displacement. This is interpreted as the fault associated with the penultimate earthquake, which happened any time after the deposition of the sandy gravel layer (Unit 3). The northwestern strand exhibits a larger scarp (up to 25 cm) than

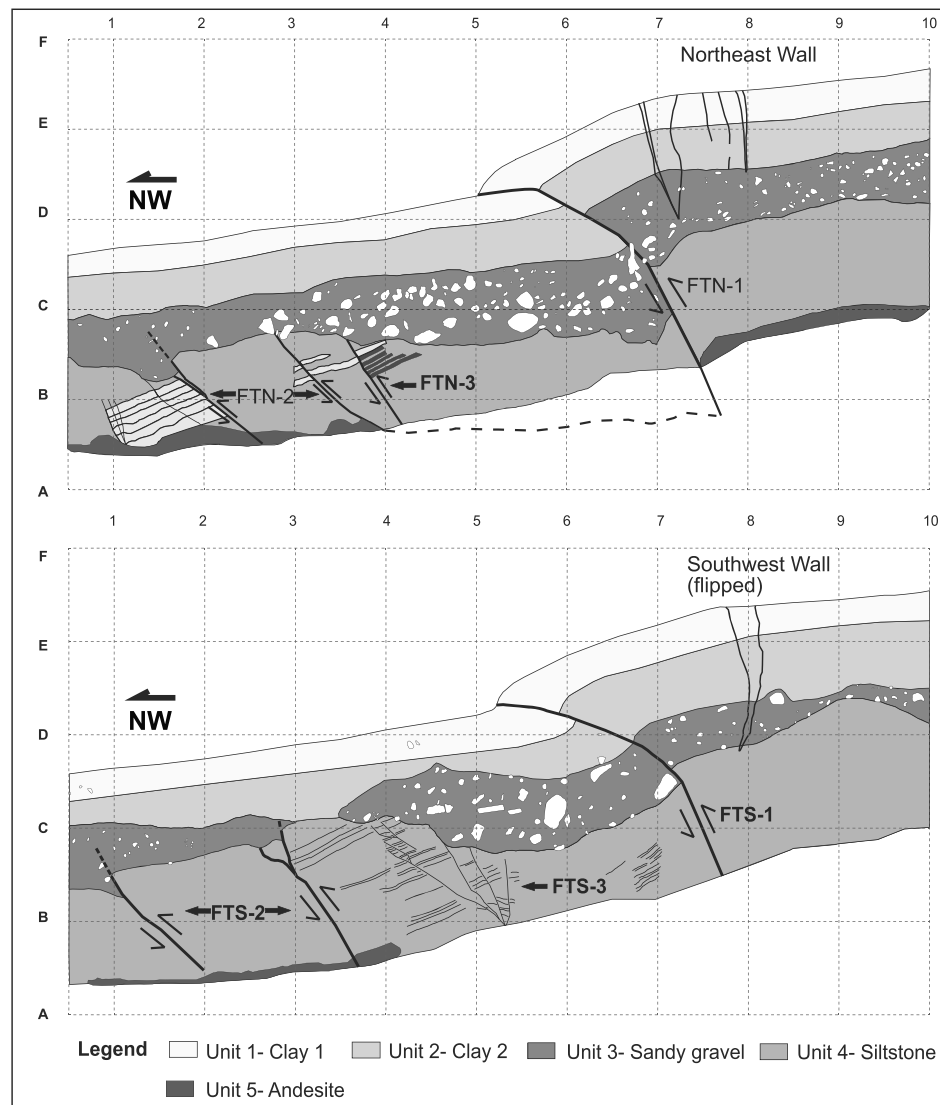


Figure 12. Tangob Trench interpretation. Grids are spaced 1 m. See supporting information Figure S20 for photomosaic.

the southeastern strand (~10 cm). The preservation of a scarp is what makes it distinct from the faults cutting only the bedrock (assigned here as Fault 3). A 25-cm-high scarp would easily be weathered and eroded if exposed on the surface for a long time; its preservation would most likely be favored by the deposition of sandy gravel layer prior to or shortly after a surface rupturing event. Fault 3 (“FTN-3” or “FTS-3”), the oldest identifiable earthquake event in this trench is represented by branching fault strands, which cut the bedrock unit (Figure 12). Faults are identified by the presence of displaced beds of siltstone and sandstone, which are more conspicuous on the southwest trench wall. All of these terminate at the contact with the sandy gravel layer (Unit 3). The absence of scarps in the fault strands assigned as Fault 3 suggests that the surface has undergone a considerable period of erosion predating the deposition of sandy gravel layer.

4.3. Calubian Trench

The 15.5-m-long, 4.5-m-deep, and 3-m-wide single-slot-style Calubian Trench was excavated across two fault scarps: a 1.5-m-high sinistral pressure-ridge fault scarp and a 0.15-m monoclinial fault scarp.

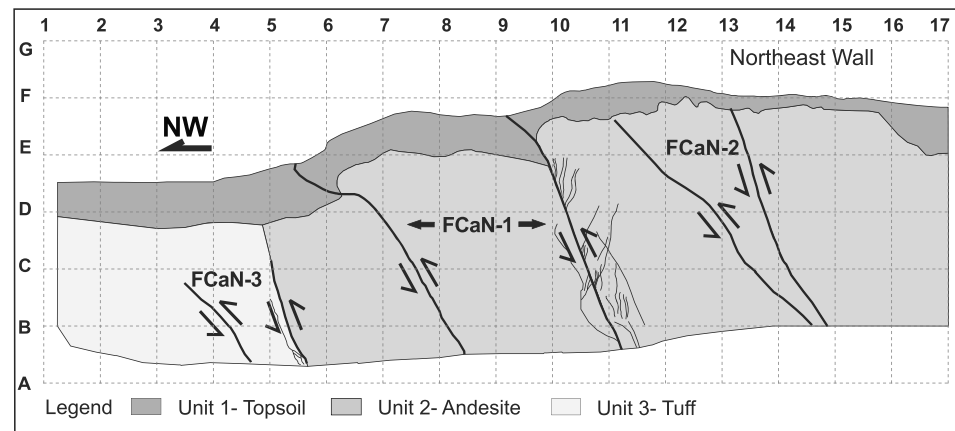


Figure 13. Calubian Trench interpretation. Grids are spaced 1 m. See supporting information Figure S21 for photomosaic.

4.3.1. Stratigraphy of Calubian Trench

Three stratigraphic units were identified in this trench. Two units are unconsolidated deposits, while the third oldest is bedrock. The units are described in detail in order of relative age (Unit 1 being the youngest unit; Figure 13). For this trench, only the northeastern wall is shown for brevity.

Unit three (3) is highly weathered andesite bedrock (Figure 13). Unit 2 is a fine-grained volcanoclastic rock identified as tuff. Unit 1 is topsoil. The soil cover in Calubian Trench is relatively poorly developed compared to the soil profile observed in the Luwak and Tangob Trenches. The only soil horizon formed in the Calubian Trench is topsoil, which is followed immediately by bedrock (Figure 13). No sandy gravel layer similar to Unit 3 in the Tangob and Luwak Trenches was found. The soil layer can be as thin as 20 cm but reaches about 50 cm on the downthrown block. No organic material was recovered from this layer.

4.3.2. Evidence of Faulting

Fault 1 (“FCaN-1” in Figure 13) pertains to the 2013 event, which is associated with two main fault strands and which produced two individual scarps. The northwest scarp, which shows larger displacement, is associated with a fault strand that dips 60°SE in Unit 2 and shallows to 30°SE in Unit 1. This fault strand produced a scarp approximately 1 m high. The other major strand of Fault 1 to the southeast dips 70°SE in Unit 1 and shallows to 50°SE and produced a scarp approximately 50 cm high (Figure 13). Fault 2 (“FCaN-2” in Figure 13), the strands which terminate at the interface between the andesite and the topsoil, is attributed to the penultimate event. The fault strand to the northwest dips 50°SE and the strand to the southeast dips 70°SE. These strands seem to bifurcate from a meter below the trench exposure. Fault 3 (“FCaN-3” in Figure 13) pertains to two fault strands that are associated with the oldest earthquake event in this trench, because these terminate abruptly within the volcanoclastic sediments rather than at the contact with the topsoil (Unit 1). The fault strand to the northwest dips 50°SE, while the fault strand to the southeast dips 70°SE (Figure 13).

4.4. Cumayot Trench

The 12.5-m-long, 5-m-deep, and 3-m-wide single-slot-style Cumayot Trench was excavated across a 2-m-high protruding monoclinical fault scarp.

4.4.1. Stratigraphy of Cumayot Trench

Only two stratigraphic units were identified in both trench walls. Unit 2 is the andesite bedrock. The andesite bedrock on the upthrown block is characterized by andesitic lava flow structures which are oriented N75°W, 45°SW. These lava flow structures are more prominent on the northeast wall (Figure 14). Unit 1 is soil cover.

4.4.2. Evidence of Faulting

Fault 1 (“FCuN-1” in Figure 14) pertains to the 2013 event, which is defined by the fault strand which is oriented N40°E, 50°SE and branches out to another strand dipping 60°SE. Movement along this fault produced a scarp of approximately 1.5 m. The tips of the linear andesitic lava flow structures near the surface which are oriented N75°W, 45°SW noticeably bend inward at the top. This is characterized as drag due to

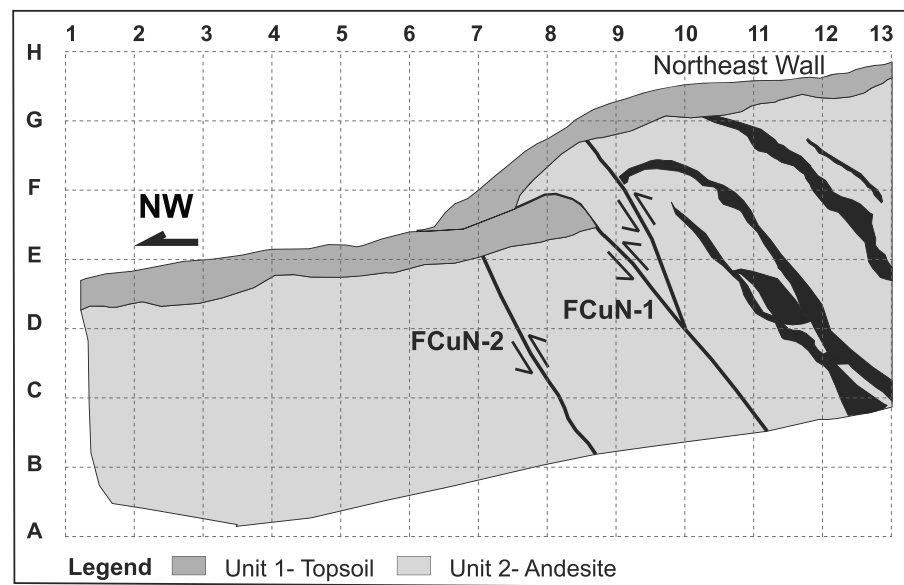


Figure 14. Cumayot Trench interpretation. Grids are spaced 1 m. See supporting information Figure S22 for photomosaic.

movement along FCuN-1. Fault 2 (“FCuN-2” in Figure 14) is the fault strand, oriented N45°E, 60°SE, that cuts through the bedrock and terminates at the interface between the bedrock and the topsoil. This can be correlated with FCaS-2 in the Calubian Trench, which is interpreted as the penultimate event.

5. Geologic Controls on the Location of the Rupture

The island of Bohol is characterized by extensive folding. A zone of northeast-southwest trending alternating anticlines and synclines, which correspond to topographic highs and lows, are found spanning the areas in Bohol that are underlain mostly by late Neogene limestones (Figure 2; Bureau of Mines and Geosciences, 1987). A southwest plunging of folds and a westward younging sequence of formations is observed in Bohol Island. The Upper Cretaceous to Paleocene metamorphic and ophiolite basement is overlain by an Eocene clastic and volcanic formation. A period of magmatism in the Late Eocene to Oligocene is manifested as andesitic flows and dioritic intrusives. These rocks are exposed mostly only in the eastern half of the island and are overlain pervasively by basinal sedimentary deposits from the Miocene to Pleistocene (Mines and Geosciences Bureau, 2010; Figure 2).

Cross section A–A′ (Figure 15a) shows gently folded Middle Miocene clastics and limestones and Pliocene clastics and limestones. That the rupture coincides with older gentle folding suggests the presence of what may have originally been a fault-propagation fold that eventually ruptured certain portion of Bohol's northern coastline.

Cross section B–B′ (Figure 15b) shows that the rupture coincides with the steeply dipping beds of folded Early to Middle Eocene sedimentary sequences and volcanic rocks in the northern sector of the island. The rupture appears to have followed preexisting zones of weaknesses, such as contacts and/or bedding planes, as seen in some of the trenches (Figures 13 and 14). This cross section also highlights the extensive folding of the Middle Miocene clastics and limestone, Late Miocene Limestone, and Pliocene clastics and limestone in the southeastern sector of the island. Folds to the southeast of the NBF are possibly also fault-related-folding (exact location and orientation of underlying faults still unknown) resulting from regional NW-SE shortening in the Visayan Sea Basin.

Offshore 3-D seismic reflection industry survey data are available to the southwest of the onshore earthquake uplift zone. From this, two pre-2013 3-D seismic profiles were selected for analysis in this study (Arbitrary seismic lines X and Y, Figures 16a and 16b). These seismic profiles are oriented northwest, parallel to the direction of compression of the earthquake, and pass through the Bohol Strait (between the islands of

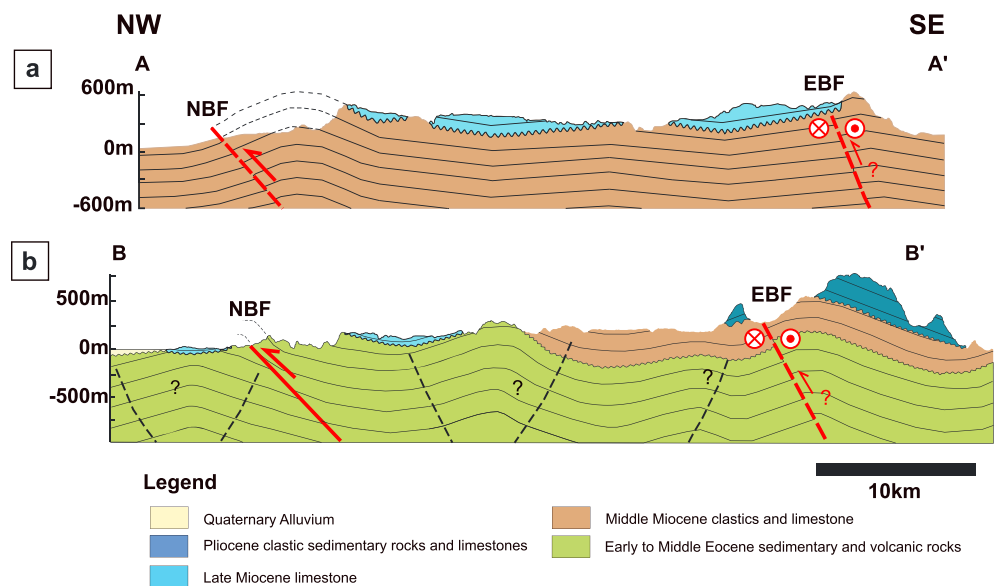


Figure 15. Geologic cross section. (a) A geologic cross section showing that the 2013 North Bohol Fault (NBF) rupture may coincide with a larger-scale fault-related folding structures, possibly explaining why rupture is sparse toward the southwest portion of the island. Kinematics of the East Bohol Fault (EBF) in the southeastern portion of the island is still uncertain. (b). A geologic cross section showing that the 2013 NBF rupture coincides with the steeply dipping beds of the Early to Middle Eocene sedimentary and volcanic rocks in the northwestern sector of the island. This section also highlights the extensive folding of the Middle Miocene to Pliocene formations in the southeastern sector of the island. Kinematics of the EBF in the southeastern portion of the island is still uncertain. Location of transects are indicated in Figure 2.

Cebu and Bohol; Figure 16c). Faults can be identified by tracing contiguously offset seismic reflectors. Arbitrary line X (Figure 16a) shows SE dipping faults that appear to cut through and terminate at the top of the seismic package equivalent to the Eocene to Oligocene clastic and volcanics. It can also be observed that these faults produced multiple event scarps of similar morphology with those found onshore. A conical structure probably corresponding to a reefal limestone growth is also seen on the upthrown footwall of the faulted block system (Figure 16a). Arbitrary line Y (Figure 16b) shows fold-thrust structures. Folds in Miocene to present clastics and limestones are rooted in NE striking SE dipping faults that cut through the erosional surface of Eocene to Oligocene clastic and volcanics. Such fold-fault structures replicate onshore observations, such as shown in Figure 15a. Thus, analysis of industry offshore seismic reflection data reveals structures that have not been presented in the context of tectonics and provide a more regional context of deformation for the NBF.

6. Discussion

6.1. Short, Discontinuous Rupture on a Previously Unmapped Fault: Combination of Surface and Blind Faulting

Active faults can go unnoticed prior to a recent earthquake due to lack of evidence for activity, such as related historical seismicity and convincing preexisting morphotectonic features (Hornblow et al., 2014). Heavy vegetation and rapid erosion can also be a hindrance to mapping already subtle tectonic landforms. In many cases, surface faulting is identified only after an earthquake with high-resolution remote sensing (e.g., LiDAR or interferometric synthetic aperture radar, InSAR) that can detect deformation features below the tree canopy (e.g., Duffy et al., 2013; Gold et al., 2013; Langridge et al., 2018; Litchfield et al., 2018; Nicol et al., 2018; and Oskin et al., 2012).

Characteristics of the various types of ground deformation observed (e.g., coastal uplift, landslide distribution, and liquefaction) suggest that deformation from the earthquake occurred along a southeast dipping reverse fault that is around 70 km long. Our field investigation shortly after the 2013 earthquake and mapping from 1-m resolution LiDAR DEM (Felix, 2017; Felix et al., 2014) made it possible to identify several

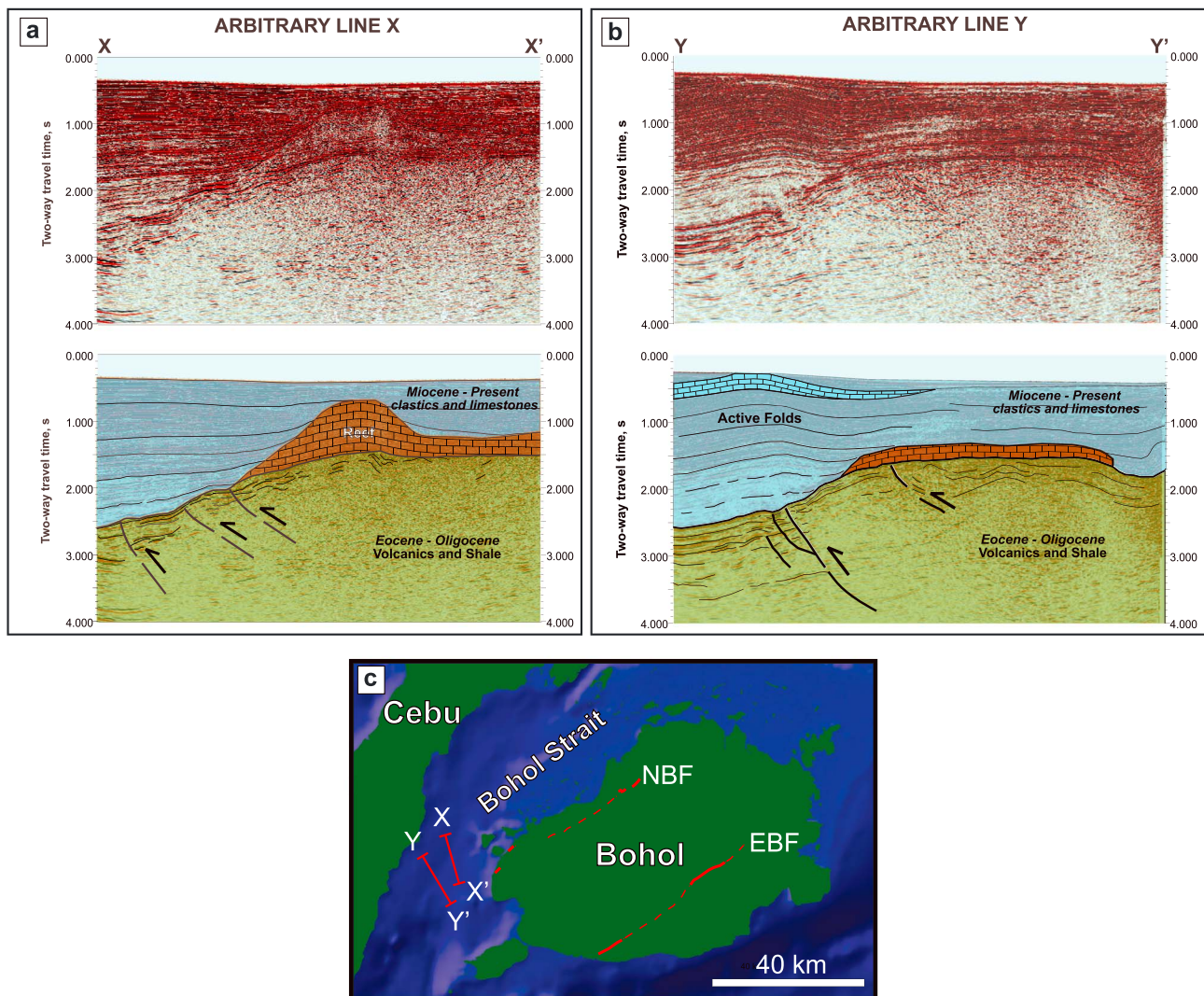


Figure 16. Pre-2013 industry acquired 3-D seismic profiles in the Bohol Strait. EBF = East Bohol Fault; NBF = North Bohol Fault.

other ground rupture traces on the southeastern portion of the island, further away from the more conspicuous surface rupture in the northeast. This corroborates observations from SAR pixel offset analysis by Kobayashi (2014), which shows a 50-km-long east-northeast trending deformation zone with ground uplift of up to more than 1 m.

The rupture mapped in this study and the short and highly discontinuous traces of the 2013 ground rupture also mapped by Felix et al. (2014) and Felix (2017) in the southeastern portion of Bohol only add up to a length of about 8 km, which is much shorter than the length of the deformation zone defined by seismicity plots (Figure 1b) and modeling from SAR data (Kobayashi, 2014). It is worth noting, however, that the maximum and average scarp heights of approximately 5 and 2 m high, are consistent with the 4.88-m maximum displacement and 2.13-m average displacement, respectively, computed from scaling relationship between earthquake magnitudes and maximum reverse fault displacement (Wells & Coppersmith, 1994).

While shorter-than-expected ruptures associated thrust/reverse earthquakes of intermediate magnitude ($\sim M_w 7$) are not uncommon (e.g., Rockwell et al., 2013; Volponi et al., 1978), a rather short and discontinuous ground rupture despite a much longer deformation zone from seismicity, SAR pixel offset analysis, and LiDAR mapping, still raises questions about the deformation style of this particular fault. Kobayashi (2014) observed a correlation between reverse-fault motion/uplift and high elevation and suggests that repeated historic movement of the NBF contributed to the existing topography of the area. In the island,

elevation highs coincide with areas underlain by anticlines (Figures 2 and 15). It is therefore possible that the limited ground surface faulting expression accompanying the earthquake could be due to fault slip not reaching the surface (“blind faulting”) but still contributing to the growth of the folds (e.g., Ainscoe et al., 2017). Folding may still accommodate northwest-southeast shortening in some parts of the northern coastal areas of Bohol and may explain the discontinuity of the 2013 coseismic ground rupture. A long recurrence interval (as discussed in section 7.2), which may possibly explain the few events identified in the trench, could also be due to distribution of strain among many structures in a wide fold-and-thrust belt, as shown by the results of geologic mapping and interpreting offshore seismic profiles (Figures 15 and 16).

6.2. Potential Prehistoric Earthquakes

In addition to the geologic and geodetic observations, paleoseismic investigation indicates the presence of several older fault strands alongside the 2013 earthquake fault plane. From the trenching exposures (Figures 10 and 12–14), at least two possible pre-2013 events were identified. Despite the presence of radiocarbon dated material in Luwak Trench (Figure 10), the limited stratification and poor preservation of cross-cutting relationships in the Luwak Trench prevented placing proper constraints on the timing of events associated with the NBF. For instance, FLN-2 and FLN-3, although terminating at contacts between different strata, both only cut bedrock and therefore could not be reliably distinguished. On the other hand, in the Tangob Trench, while what appear to be the counterparts of the Luwak Trench fault strands FLN-2 and FLN-3 (faults FTN-2/FTS-2 and FTN-3/FTS-3) can be confidently distinguished as two different events, there are no datable materials to constrain their ages. However, if the sandy gravel layer units (“Unit 3”) in both trenches can be correlated, then it is possible that at least one pre-2013 event may have happened in the past ~12,000 years because faulting event number 2 represented by FLN-2 and FTS-2/FTN-2 in Figures 10 and 12, respectively, traverses this gravel unit (see also Table 1).

While the trenches seem to suggest the occurrence of at least one and up to two pre-2013 events in the Holocene, there are likely more earthquake events that may not have manifested or been preserved in the location of the trench exposures. This could be attributed to a relatively wide deformation zone of distributed reverse faulting and shortening (e.g., the approximately 50-m-wide zone of left-stepping 1.5-m-high fault scarps of the most recent earthquake in Sitio Calubian, Barangay Anonang, seen in Figure 8e). Considering the limited length of the trenches (maximum of 15 m), some events may have been missed out. Another possible reason for the oversight of other fault strands associated to earthquake events in the trench walls is the variable, discontinuous and irregular surface rupture behavior characteristic of reverse faults. It is very likely that not all similar magnitude earthquake events are expressed in the trenches because the NBF may have not ruptured along the same segment or to the ground surface during some of the previous earthquake events. The lack of stratification due to high erosion rates in the area may also be contributory to lack of preservation of earthquake event horizons in the trenches. Each of the several fault strands seen cutting through bedrock, especially in the Luwak Trench, could possibly be attributed to separate earthquake events. The ages of the individual fault strands could have possibly been constrained had the stratification been more well developed.

From an archaeoseismological point of view, the age of the oldest church in Bohol (the Church of Our Lady of the Immaculate Conception in Baclayon; built in 1595 AD), which was destroyed during the 2013 earthquake, can provide additional, off-fault constraints for the occurrence/nonoccurrence of a similar magnitude earthquake possibly caused by the NBF. Since there are no reports of similar damage to this church since it was built, it is possible that 418 years before 2013, there have been no similarly large-magnitude earthquakes on faults close enough to Baclayon (including the NBF) that may have caused the same intensity of shaking that destroyed it in 2013.

7. Conclusions

The M_w 7.2 2013 Bohol earthquake occurred as a consequence of northwest-southeast shortening, resulting from relative motion between the Sunda Plate and the Visayan basin in the Philippine mobile belt. It revealed a previously unmapped NBF. Seismicity, ground rupture patterns, scarp morphologies, and fault geometry from trench exposures of the ground rupture associated with the earthquake are all consistent with a NE trending, SE dipping NBF, which has a predominantly reverse-slip component of movement.

Short, discontinuous rupture could possibly be a result of a combination of surface and blind faulting. In the trenches, at least one, and possibly two, pre-2013 surface rupturing earthquakes of similar magnitude were identified. The few events identified (and long recurrence intervals) may be a result of shortening being distributed among many faults and folds across the island.

The appearance of the ground rupture along the previously unmapped NBF underscores the importance of reviewing our method for identifying and delineating active faults. In mapping active faults in settings similar to the Philippines, it might be beneficial to use more relaxed criteria for identifying Quaternary-active faults—which is not only based on detecting more obvious offset on more recent Quaternary features such as alluvial fans and offset channels—but also looking into subtle longer-term Quaternary morphotectonic features such as faceted spurs and cumulative scarps on bedrock hillslopes, oversteepened mountain fronts, and landslide or talus alignments, among others (Lettis et al., 1997; Slemmons, 1977).

The discovery of the NBF is key in understanding the seismotectonic setting of the Visayan region. Fault-fold structures, which were identified from analysis of offshore seismic reflection profiles in the Bohol strait and from onshore geological transect to provide a broader tectonic context for the NBF, also seem to play a large role in accommodation of deformation from the northwest-southeast shortening governing the actively deforming Visayan Sea Basin (Aurelio et al., 2015; Rangin et al., 1989). Therefore, there are still a lot of onshore and offshore structures within the vicinity of the NBF that need to be investigated for their seismic potential.

Acknowledgments

We thank the Office of the Vice Chancellor for Research and Development (OVCRD) of the University of the Philippines-Diliman for funding this study, which is part of the project Seismotectonics of the Magnitude 7.2 Bohol earthquake of 15 October 2013: Implications to Earthquake Hazard Assessment in Metro Manila (Project 131308 SOS). We also gratefully acknowledge Bohol Governor Edgardo Chatto, Inabanga Mayor Josephine Socorro “Roygie” Jumamoy, and all the Inabanga Municipal staff for logistical support during the study. LiDAR data are courtesy and copyright of the Phil-LiDAR (Philippine-Light Detection and Ranging) Program and DREAM (Disaster Risk and Exposure Assessment for Mitigation) Program. All Rights Reserved while seismic profiles are courtesy of PetroEnergy Resources Corporation. Many thanks to Editor Taylor Schildgen and two anonymous reviewers for their very constructive and useful comments. Photos of locations of scarp height measurements, scarp topographic profiles, trench photomosaics, and C-14 calibration data can be found in the supporting information.

References

- Acharya, H. K., & Aggarwal, Y. P. (1980). Seismicity and tectonics of the Philippine Islands. *Journal of Geophysical Research*, 85(B6), 3239–3250. <https://doi.org/10.1029/JB085iB06p03239>
- Ainscoe, E. A., Abdrakhmatov, K. E., Baikulov, S., Carr, A. S., Elliott, A. J., Grützner, C., & Walker, R. T. (2018). Variability in surface rupture between successive earthquakes on the Susamyr Fault, Kyrgyz Tien Shan: implications for palaeoseismology. *Geophysical Journal International*, 216(1), 703–725.
- Ainscoe, E. A., Elliott, J. R., Copley, A., Craig, T. J., Li, T., Parsons, B. E., & Walker, R. T. (2017). Blind thrusting, surface folding, and the development of geological structure in the Mw 6.3 2015 Pishan (China) earthquake. *Journal of Geophysical Research: Solid Earth*, 122, 9359–9382. <https://doi.org/10.1002/2017JB014268>
- Allen, C. R. (1962). Circum-Pacific faulting in the Philippines-Taiwan region. *Journal of Geophysical Research*, 67(12), 4795–4812. <https://doi.org/10.1029/JZ067i012p04795>
- Aurelio, M. (2000a). Shear partitioning in the Philippines: Constraints from Philippine Fault and global positioning system data. *Island Arc*, 9(4), 584–597. <https://doi.org/10.1046/j.1440-1738.2000.00304.x>
- Aurelio, M. A. (2000b). Tectonics of the Philippines revisited. *Journal of the Geological Society of the Philippines*, 55, 119–183.
- Aurelio, M., Barrier, E., Gaulon, R., & Rangin, C. (1997). Deformation and stress states along the central segment of the Philippine Fault: Implications to wrench tectonics. *Journal of Asian Earth Sciences*, 15, 107–119.
- Aurelio, M., Barrier, E., Rangin, C., & Muller, C. (1991). The Philippine Fault in the late Cenozoic evolution of the Bondoc-Masbate-N. Leyte area, central Philippines. *Journal of Southeast Asian Earth Sciences*, 6(3-4), 221–238. [https://doi.org/10.1016/0743-9547\(91\)90069-A](https://doi.org/10.1016/0743-9547(91)90069-A)
- Aurelio, M., Huchon, P., Barrier, E., & Gaulon, R. (1994). Displacement rates along the Philippine Fault estimated from slip-vectors and regional kinematics. *Journal of the Geological Society of the Philippines*, 49, 65–77.
- Aurelio, M. A., Taguiba, K. L. P., Dianala, J. D. B., Rimando, J. M., & Urquico-Zalcita, J. C. D. 2015. Active tectonic deformation of the Visayan Basin (Philippines): Insights from the twin earthquakes of Negros (Mw 6.9, 2012) and Bohol (Mw 7.2, 2013), In: Proceedings crust mantle evolution in active arcs, Quezon City, Philippines.
- Bacolcol, T., Cahulogan, M., Punongbayan, B. J., Evangelista, N., Hernandez, V., Bariso, E., et al., 2013. Geologic impacts of the 15 October 2013 Mw 7.2 North Bohol Fault earthquake, Bohol Island, In: Proceedings GEOCON 2013: The 26th Annual Geological Convention, Makati City, Philippines.
- Barrier, E., Huchon, P., & Aurelio, M. (1991). Philippine Fault: A key for Philippine kinematics. *Geology*, 19(1), 32–35. [https://doi.org/10.1130/0091-7613\(1991\)019<0032:PPFAKFP>2.3.CO;2](https://doi.org/10.1130/0091-7613(1991)019<0032:PPFAKFP>2.3.CO;2)
- Bautista, B. C., Bautista, M. L. P., Oike, K., Wu, F. T., & Punongbayan, R. S. (2001). A new insight on the geometry of subducting slabs in northern Luzon, Philippines. *Tectonophysics*, 339(3-4), 279–310. [https://doi.org/10.1016/S0040-1951\(01\)00120-2](https://doi.org/10.1016/S0040-1951(01)00120-2)
- Besana, G. M., & Ando, M. (2005). The central Philippine Fault Zone: Location of great earthquakes, slow events, and creep activity. *Earth Planets Space*, 57(10), 987–994. <https://doi.org/10.1186/BF03351877>
- Bischke, R., Suppe, J., & Del Pilar, R. (1990). A new branch of the Philippine fault system as observed from aeromagnetic and seismic data. *Tectonophysics*, 183(1-4), 243–264. [https://doi.org/10.1016/0040-1951\(90\)90419-9](https://doi.org/10.1016/0040-1951(90)90419-9)
- Bronk Ramsey, C. (2009). Bayesian analysis of radiocarbon dates. *Radiocarbon*, 51(1), 337–360. <https://doi.org/10.1017/s003822200033865>
- Bureau of Mines and Geosciences (1987). Geologic maps of Bohol Island. Bureau of Mines and Geosciences Philippines. Department of Environment, Energy and Natural Resources.
- Cardwell, R. K., Isacks, B. L., & Karig, D. E. (1980). The spatial distribution of earthquakes, focal mechanism solutions, and subducted lithosphere in the Philippine and northeastern Indonesian Islands. In D. E. Hayes (Ed.), *The tectonic and geologic evolution of Southeast Asian seas and islands* (pp. 1–35). Washington, DC: American Geophysical Union. <https://doi.org/10.1029/GM023p0001>
- Daligdig, J. A. (1997). *Recent faulting and paleoseismicity along the Philippine fault zone, north central Luzon, Philippines*, Ph.D. thesis. Kyoto, Japan: Faculty of Science, Kyoto University.

- Duffy, B., Quigley, M., Barrell, D. J., Van Dissen, R., Stahl, T., Leprince, S., et al. (2013). Fault kinematics and surface deformation across a releasing bend during the 2010 M_W 7.1 Darfield, New Zealand, earthquake revealed by differential LiDAR and cadastral surveying. *Bulletin*, 125(3-4), 420–431.
- Dziewonski, A. M., Chou, T.-A., & Woodhouse, J. H. (1981). Determination of earthquake source parameters from waveform data for studies of global and regional seismicity. *Journal of Geophysical Research*, 86(B4), 2825–2852. <https://doi.org/10.1029/JB086iB04p02825>
- Ekström, G., Nettles, M., & Dziewoński, A. M. (2012). The global CMT project 2004–2010: Centroid-moment tensors for 13,017 earthquakes. *Physics of the Earth and Planetary Interiors*, 200–201, 1–9. <https://doi.org/10.1016/j.pepi.2012.04.002>
- Felix, R. (2017). *Morphotectonic analysis of the North Bohol Fault in Bohol, Philippines using high-resolution topographic models and field analysis*. M.Sc. thesis, (p. 169). Diliman, Quezon City, Philippines: National Institute of Geological Sciences, College of Science, University of the Philippines.
- Felix, R., Lagmay, A. M. F., Norini, G., & Eco, R. (2014). Mapping of the Inabanga Fault in Bohol, Philippines using high resolution LIDAR imagery and field mapping verification. In: Proceedings 5th International Union for Quaternary Science Meeting on Paleoseismology, Active Tectonics and Archeoseismology (PATA), Busan, South Korea.
- Gold, R. D., Stephenson, W. J., Odum, J. K., Briggs, R. W., Crone, A. J., & Angster, S. J. (2013). Concealed Quaternary strike-slip fault resolved with airborne lidar and seismic reflection: The Grizzly Valley fault system, northern Walker Lane, California. *Journal of Geophysical Research: Solid Earth*, 118, 3753–3766. <https://doi.org/10.1002/jgrb.50238>
- Hamburger, M., Cardwell, R., & Isacks, B. (1983). Seismotectonics of the Luzon, Philippines, region. In D. E. Hayes (Ed.), *The tectonic and geologic evolution of Southeast Asian seas and islands*, (pp. 1–35). Washington, D.C.: American Geophysical Union. <https://doi.org/10.1029/GM027p0001>
- Hamilton, W. B., 1979. Tectonics of the Indonesian region, Professional Paper, 345pp.
- Hardebeck, J. L., & Shearer, P. M. (2002). A new method for determining first-motion focal mechanisms. *Bulletin of the Seismological Society of America*, 92(6), 2264–2276. <https://doi.org/10.1785/0120010200>
- Hayes, D. E., & Lewis, S. D. (1985). Structure and tectonics of the Manila Trench System, western Luzon, Philippines. *Energy*, 10(3-4), 263–279. [https://doi.org/10.1016/0360-5442\(85\)90046-5](https://doi.org/10.1016/0360-5442(85)90046-5)
- Hornblow, S., Quigley, M., Nicol, A., Van Dissen, R., & Wang, N. (2014). Paleoseismology of the 2010 M_W 7.1 Darfield (Canterbury) earthquake source, Greendale Fault, New Zealand. *Tectonophysics*, 637, 178–190. <https://doi.org/10.1016/j.tecto.2014.10.004>
- Kaneda, H., Nakata, T., Tsutsumi, H., Kondo, H., Sugito, N., Awata, Y., et al. (2008). Surface rupture of the 2005 Kashmir, Pakistan, earthquake and its active tectonic implications. *Bulletin of the Seismological Society of America*, 98(2), 521–557. <https://doi.org/10.1785/0120070073>
- Kobayashi, T. (2014). Remarkable ground uplift and reverse fault ruptures for the 2013 Bohol earthquake (M_W 7.1), Philippines, revealed by SAR pixel offset analysis. *Geoscience Letters*, 1, 1–7.
- Lagmay, A. M. F., & Eco, R. (2014). Brief communication: On the source characteristics and impacts of the magnitude 7.2 Bohol earthquake, Philippines. *Natural Hazards and Earth System Sciences*, 14(10), 2795–2801. <https://doi.org/10.5194/nhess-14-2795-2014>
- Langridge, R. M., Rowland, J., Villamor, P., Mountjoy, J., Townsend, D. B., Nissen, E., et al. (2018). Coseismic rupture and preliminary slip estimates for the Papatea Fault and its role in the 2016 M_W 7.8 Kaikōura, New Zealand, earthquake. *Bulletin of the Seismological Society of America*, 108(3B), 1596–1622. <https://doi.org/10.1785/0120170336>
- Lettis, W. R., Wells, D. L., & Baldwin, J. N. (1997). Empirical observations regarding reverse earthquakes, blind thrust faults, and quaternary deformation: Are blind thrust faults truly blind? *Bulletin of the Seismological Society of America*, 87, 1171–1198.
- Lin, A., Ouchi, T., Chen, A., & Maruyama, T. (2001). Co-seismic displacements, folding and shortening structures along the Chelungpu surface rupture zone occurred during the 1999 Chi-Chi (Taiwan) earthquake. *Tectonophysics*, 330(3-4), 225–244. [https://doi.org/10.1016/S0040-1951\(00\)00230-4](https://doi.org/10.1016/S0040-1951(00)00230-4)
- Litchfield, N. J., Villamor, P., Dissen, R. J. V., Nicol, A., Barnes, P. M., Barrell, D. J., et al. (2018). Surface rupture of multiple crustal faults in the 2016 M_W 7.8 Kaikōura, New Zealand, earthquake. *Bulletin of the Seismological Society of America*, 108(3B), 1496–1520. <https://doi.org/10.1785/0120170300>
- Liu-Zeng, J., Zhang, Z., Wen, L., Tapponnier, P., Sun, J., Xing, X., et al. (2009). Co-seismic ruptures of the 12 May 2008, Ms 8.0 Wenchuan earthquake, Sichuan: East-west crustal shortening on oblique, parallel thrusts along the eastern edge of Tibet. *Earth and Planetary Science Letters*, 286(3-4), 355–370. <https://doi.org/10.1016/j.epsl.2009.07.017>
- Metal Mining Agency of Japan-Japan International Cooperation Agency (1985). 1:250,000 Geologic map of the Bohol-Siquijor area in the mineral exploration—Mineral deposits and tectonics of two contrasting geological environments in the Republic of the Philippines, Phase I.
- Mines and Geosciences Bureau (MGB) (2010). *Geology of the Philippines* (2nd ed.). Quezon City, Philippines: Mines and Geosciences Bureau, Department of Environment and Natural Resources.
- Nakata, T., Sangawa, A., & Hirano, S. (1977). A report on tectonic landforms along the Philippine fault zone in Northern Luzon, Philippines, Science Reports of the Tohoku University. *Seventh Series (Geography)*, 7, 69–93.
- Nakata, T., Tsutsumi, H., Punongbayan, R. S., Rimando, R. E., Daligdig, J. A., Daag, A.S., Besana, G. M. (1996). Surface fault ruptures of the 1990 Luzon earthquake, Philippines. Hiroshima University-Research Center for Regional Geography Special Publication No. 25.
- National Research Institute for Earth Science and Disaster Resilience (NIED) (2013). <http://www.isn.bosai.go.jp/events/20131015001235/index.html>. Accessed 18 Oct 2013.
- Nicol, A., Khajavi, N., Pettinga, J. R., Fenton, C., Stahl, T., Bannister, S., et al. (2018). Preliminary geometry, displacement, and kinematics of fault ruptures in the epicentral region of the 2016 M_W 7.8 Kaikōura, New Zealand, earthquake. *Bulletin of the Seismological Society of America*, 108(3B), 1521–1539. <https://doi.org/10.1785/0120170329>
- Oskin, M. E., Arrowsmith, J. R., Corona, A. H., Elliott, A. J., Fletcher, J. M., Fielding, E. J., et al. (2012). Near-field deformation from the El Mayor-Cucapah earthquake revealed by differential LIDAR. *Science*, 335(6069), 702–705. <https://doi.org/10.1126/science.1213778>
- Ozawa, A., Tagami, T., Listanco, E. L., Arpa, C. B., & Sudo, M. (2004). Initiation and propagation of subduction along the Philippine Trench: Evidence from the temporal and spatial distribution of volcanoes. *Journal of Asian Earth Sciences*, 23(1), 105–111. [https://doi.org/10.1016/S1367-9120\(03\)00112-3](https://doi.org/10.1016/S1367-9120(03)00112-3)
- Philip, H., Rogozhin, E., Cisternas, A., Bousquet, J. C., Borisov, B., & Karakhanian, A. (1992). The Armenian earthquake of 1988 December 7: Faulting and folding, neotectonics and palaeoseismicity. *Geophysical Journal International*, 110(1), 141–158. <https://doi.org/10.1111/j.1365-246X.1992.tb00718.x>
- Philippine Institute of Volcanology and Seismology (PHIVOLCS) (2008). Distribution of active faults and trenches in the Philippines map. Accessed: 21 Sept 2014. (http://www.phivolcs.dost.gov.ph/index.php?option=com_content&view=article&id=78&Itemid=500024)

- Philippine Institute of Volcanology and Seismology (PHIVOLCS) (2014). Latest earthquake information. <http://earthquake.phivolcs.dost.gov.ph>. Accessed: 12 May 2014
- Pubellier, M., Deffontaines, B., Quebral, R., & Rangin, C. (1994). Drainage network analysis and tectonics of Mindanao, southern Philippines. *Geomorphology*, 9(4), 325–342. [https://doi.org/10.1016/0169-555X\(94\)90053-1](https://doi.org/10.1016/0169-555X(94)90053-1)
- Quebral, R. D., Pubellier, M., & Rangin, C. (1996). The onset of movement on the Philippine Fault in eastern Mindanao: A transition from a collision to a strike-slip environment. *Tectonics*, 15(4), 713–726. <https://doi.org/10.1029/95TC00480>
- Rangin, C., Porth, H., & Müller, C. (1989). Neogene geodynamic evolution of the Visayan Region. *Geologisches Jahrbuch*, 70, 7–27.
- Reimer, P. J., Bard, E., Bayliss, A., Beck, J. W., Blackwell, P. G., Bronk Ramsey, C., et al. (2013). IntCal13 and Marine13 radiocarbon age calibration curves 0–50,000 years cal BP. *Radiocarbon*, 55(4), 1869–1887. https://doi.org/10.2458/azu_js_rc.55.16947
- Reimer, P. J. (2004). *IntCal04. Radiocarbon*, 46(3), 1029–1058.
- Rimando, J. M. (2015). *Ground deformation associated with the October 15, 2013 magnitude (MW) 7.2 Bohol earthquake, Bohol Island, Philippines*, M.Sc. thesis, (p. 129). Diliman, Quezon City, Philippines: National Institute of Geological Sciences, College of Science, University of the Philippines.
- Rimando, R. E., & Knuepfer, P. L. K. (2006). Neotectonics of the Marikina Valley fault system (MVFS) and tectonic framework of structures in northern and central Luzon, Philippines. *Tectonophysics*, 415(1–4), 17–38. <https://doi.org/10.1016/j.tecto.2005.11.009>
- Ringenbach, J. C., Pinet, N., Stephan, J. F., & Delteil, J. (1993). Structural variety and tectonic evolution of strike-slip basins related to the Philippine Fault System, Northern Luzon, Philippines. *Tectonics*, 12(1), 187–203. <https://doi.org/10.1029/92TC01968>
- Rockwell, T. K., Ragona, D. E., Meigs, A. J., Owen, L. A., Costa, C. H., & Ahumada, E. A. (2013). Inferring a thrust-related earthquake history from secondary faulting: A long rupture record of La Laja Fault, San Juan, Argentina. *Bulletin of the Seismological Society of America*, 104(1), 269–284.
- Slemmons, D. B., 1977. Faults and earthquake magnitude: U. S. Army Engineers Waterways Experiment Station, Vicksburg, Miss., Miscellaneous Paper S-73-1, Report 6, 166 p.
- Tan, X., Yuan, R., Xu, X., Chen, G., Klinger, K., Chang, C., et al. (2012). Complex surface rupturing and related formation mechanisms in the Xiaoyudong area for the 2008 Mw 7.9 Wenchuan earthquake, China. *Journal of Asian Earth Sciences*, 58, 132–142. <https://doi.org/10.1016/j.jseas.2012.06.005>
- Tape, W., & Tape, C. (2012). A geometric setting for moment tensors. *Geophysical Journal International*, 190(1), 476–498. <https://doi.org/10.1111/j.1365-246X.2012.05491.x>
- Tsutsumi, H., Perez, J. S., Marjes, J. U., Papiona, K. L., & Ramos, N. T. (2015). Coseismic Displacement and Recurrence Interval of the 1973 Ragay Gulf earthquake, Southern Luzon, Philippines. *Journal of Disaster Research*, 10(1), 83–90. <https://doi.org/10.20965/jdr.2015.p0083>
- U.S. Geological Survey (USGS) (2013). M7.1-5km SE of Sagbayan, Philippines (BETA). <https://earthquake.usgs.gov/earthquakes/event-page/usb000kdb4#executive>. Accessed: 20 Nov 2013.
- University of the Philippines Training Center for Applied Geodesy and Photogrammetry, 2015. DREAM LiDAR data acquisition and processing for Bohol River Floodplain, Disaster Risk and Exposure Assessment for Mitigation (DREAM), DOST Grants-In-Aid Program, 72pp. Accessed from <https://lipad.dream.upd.edu.ph/documents/3627> on 17 September 2018.
- Vallage, A., Klinger, Y., Grandin, R., Bhat, H. S., & Pierrot-Deseilligny, M. (2015). Inelastic surface deformation during the 2013 Mw 7.7 Balochistan, Pakistan, earthquake. *Geology*, 43(12), 1079–1082.
- Volponi, F., Quiroga, M., Robles, A., & Sisterna, J. (1978). El terremoto de Cauete del 23 de noviembre de 1977. Instituto Sismológico Zonda. Universidad Nacional de San Juan, 81.
- Wells, D., & Coppersmith, K. (1994). New empirical relationships among magnitude, rupture length, rupture width, rupture area, and surface displacement. *Bulletin of the Seismological Society of America*, 84, 974–1002.
- Yang, X., Li, W., & Qin, Z. (2015). Calculation of reverse-fault-related parameters using topographic profiles and fault bedding. *Geodesy and Geodynamics*, 6(2), 106–112. <https://doi.org/10.1016/j.geog.2014.09.002>
- Yu, S. B., Hsu, Y. J., Bacolcol, T., Yang, C. C., Tsai, Y. C., & Solidum, R. (2013). Present-day crustal deformation along the Philippine Fault in Luzon, Philippines. *Journal of Asian Earth Sciences*, 65, 64–74. <https://doi.org/10.1016/j.jseas.2010.12.007>

Erratum

In the originally published version of this article, “SAR pixel offset analysis” was erroneously cited as “InSAR” in the key points and section 6.1. The article has since been corrected, and this version may be considered the authoritative version of record.